CHALMERS
UNIVERSITY OF TECHNOLOGY

Main Bearing Support Investigation

A Comparison of Wear and Friction Losses for Different Design Proposals

Master's thesis in Master Programme Applied Mechanics

TIM GYNNING OLOFSSON

Department of Applied Mechanics
CHALMERS UNIVERSITY OF TECHNOLOGY
Gothenburg, Sweden 2017

Master's thesis 2017:05

Main Bearing Support Investigation

A Comparison of Wear and Friction Losses for Different Design Proposals

TIM GYNNING OLOFSSON

Department of Applied Mechanics
Division of Dynamics
Chalmers University of Technology
Gothenburg, Sweden 2017

Main Bearing Support Investigation
A Comparison of Wear and Friction Losses for Different Design Proposals
TIM GYNNING OLOFSSON

Supervisor: Stefan Larzenius, Volvo Car Corporation
Examiner: Mikael Enelund, Department of Applied Mechanics

Master's Thesis 2017:05
Department of Applied Mechanics
Division of Dynamics
Chalmers University of Technology
SE-412 96 Gothenburg
Telephone +46 31 772 1000

Typeset in LaTeX
Printed by [Name of printing company]
Gothenburg, Sweden 2017

Main Bearing Support Investigation
A Comparison of Wear and Friction Losses for Different Design Proposals
TIM GYNNING OLOFSSON
Department of Applied Mechanics
Chalmers University of Technology

Abstract

Volvo Car Corporation uses a new generation of four cylinder inline engines in their automobiles. The engine family is known as *Volvo Engine Architecture* and the differences between the different engines are the different power outputs made possible with different engine boosts. The VEA engines utilise a bedplate design for their engines where the main bearing supports are casted into the bedplate. For the high performance engines the main bearing supports need to be sprayed with an aluminium alloy to get a strong bonding with the bedplate. The spraying is, however, expensive and an alternative solution is sought.
Four design proposals, which are based on the current design of the main bearing supports, were proposed. These design proposals does not use any of the sprayed aluminium alloy material. Instead they have been designed with the goal of getting a mechanical bonding, instead of the chemical bonding that the aluminium alloy coating provides. The design proposals were evaluated by static simulations and dynamic simulations to investigate the influence on the main bearings in terms of:

- radial deformations of the main bearing profiles,
- total pressure and asperity contact pressure and
- friction losses.

The contact behaviour between the bedplate and the main bearing supports, for the different design proposals, at high temperature were also investigated. The results from the simulations were compared to results from earlier work on the sprayed main bearing supports.
None of the design proposals generally provided lower friction losses compared to the sprayed main bearing support. The differences in friction loss should also by weighed against the potential cost saving, which is a question for VCC. The sprayed main bearing supports showed in general higher asperity contact pressure compared to the design proposals. Most of the bonding between the bedplate and the main bearing supports occurred on the top surfaces and the sides of the main bearing supports for the different design proposals. An investigation of getting fatigue failure in the bedplate should also be considered, if VCC should proceed with one or more of the design proposals.

Keywords: Aluminium alloy, Asperity contact pressure, Bedplate, Bonding, Friction losses, Main bearings, Main bearing supports, Volvo Engine Architecture.

Acknowledgements

This master's thesis was written as the final part of the master program in Applied Mechanics at Chalmers University of Technology. It has been carried out at Volvo Car Corporation Sweden in Gothenburg, during the autumn of 2016. My supervisor have been CAE engineer Stefan Larzenius who have supported me continuously throughout the project. His guidance in the use of the software *Excite PU* have also taught me a lot about dynamic simulation. I would also like to thank my examiner professor Mikael Enelund for his help and input on this thesis. I would also like to thank CAE engineer Camilla Knifsund for helping me whenever I ran into problems in *ANSA* or *ABAQUS*.

Tim Gynning Olofsson, Gothenburg, February 2017

Nomenclature

Abbreviations

CAD	Computer Aided Design
CAE	Computer Aided Engineering
DOF	Degrees of Freedom
EHD	Elasto-hydrodynamic
HD	Hydrodynamic
HP	High Performance
MB	Main Bearing
RPM	Revolutions per Minute
VCC	Volvo Car Corporation
VEA	Volvo Engine Architecture
VED	Volvo Engine Diesel

Symbols

$\bar{\beta}_{\mathrm{s}}$	Mean summit radius
$\bar{h}_{\mathrm{T}}$	Average bearing clearance gap height
δ_{s}	Roughness amplitude
$\dot{\gamma}$	Time derivative of the polar coordinate of the crank shaft displacement inside the bearing shell
$\dot{e}$	Time derivative of the polar coordinate of the crank shaft displacement inside the bearing shell
η	Dynamic lubricant viscosity
η_{s}	Summit density
γ	Polar coordinate of the crank shaft displacement
μ_{Bound}	Friction coefficient on the boundary
ν	Poisson's ratio
ω	Angular velocity
ϕ	Azimuth angle of bearing shell
σ	Composite summit roughness value

σ_{s}	Asperity summit roughness value
θ	Oil percentage gap between shell and journal
φ	Pressure flow factor
φ_{s}	Shear flow factor
A_{a}	Asperity contact area
E	Elastic modulus
e	Polar coordinate of the crank shaft displacement inside the bearing shell
E^*	Composite elastic modulus
$F_{5/2}$	Form function
F_{Bound}	Boundary force
F_{Hydro}	Hydrodynamic force
F_{Pressure}	Force from the pressure of the lubricant
F_{Shear}	Shear force
F_{Tot}	Total force
h	Nominal bearing clearance gap height
H_{s}	Dimensionless clearance parameter
h_{T}	Total clearance gap between two sliding surfaces
K	Elastic factor
N_{Bound}	Normal boundary force
N_{Bound}	Normal hydrodynamic force
N_{Tot}	Total normal force
p_{a}	Asperity contact pressure
p_{Hydro}	Hydrodynamic pressure
R	Inner shell radius

Contents

1 Introduction

This chapter will give background to the project motivating its origin and the purpose of the thesis. Delimitations and objectives are also stated in this chapter to concretize the project.

1.1 Background

In the autumn of 2013 *Volvo Car Corporation*, VCC, introduced a new engine family. These engines were designed by VCC and the engine architecture used is known as *Volvo Engine Architecture*, VEA. All the engines of the VEA-family utilise four cylinders, in-line block with different power outputs made possible with different kinds of engine boosts [1]. In VEA a bedplate design is used which means that the cylinder block is split into two separate parts (cylinder block and bedplate) with the splitting face in centre of the main bearings, see Figure 1.1.

The forces acting on the lower main bearing shells are high, therefor bearing supports are needed in the bedplate [2]. These bearing supports are made of nodular iron and casted into the high die pressure casted aluminium bedplate, see Figure 1.1. In in the high performance engines the main bearing supports are sprayed with a thin layer of an aluminium alloy to get a strong bonding with the bedplate when casted. Engines with lower power outputs use non-sprayed bearing supports, which lead to reduced bonding to the bedplate. At high temperatures, the aluminium expands more then the nodular iron which creates regions with gaps between bedplate and bearing supports. This gives less support for the main bearings and also increases the risk for fatigue problems in the bedplate.

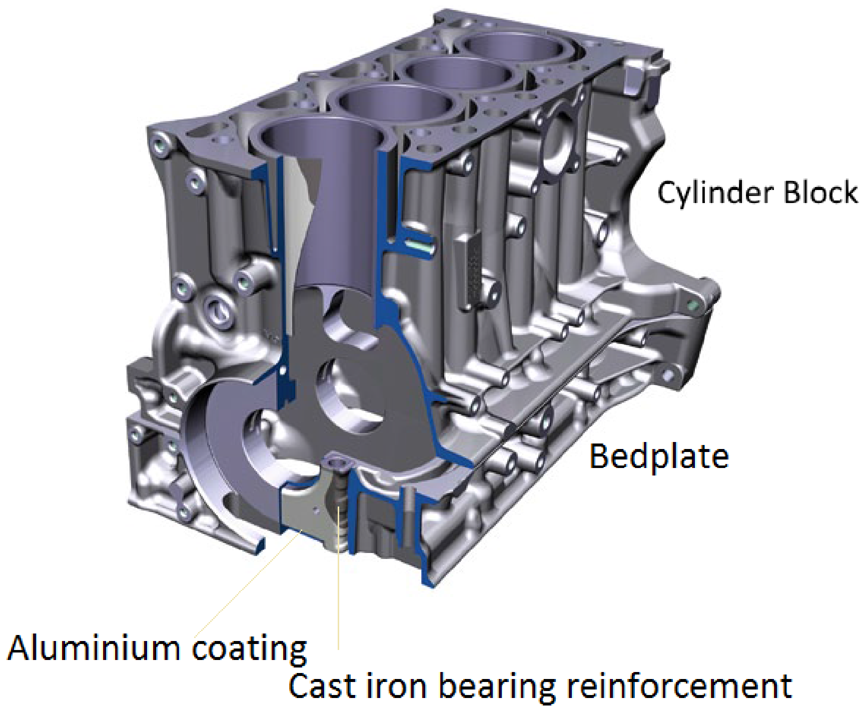

Figure 1.1: Cylinder block with bedplate with a cutaway revealing the cast iron bearing reinforcements [1].

In order to investigate how large the differences are in friction losses and asperity contact pressure between non-sprayed main bearing supports and sprayed main bearing supports when used in the high performance engines a number of analyses were performed at VCC [3]. From the investigation a number of conclusions were drawn

- The bonding between non-sprayed bearing supports and bedplate has strong impact on the radial deformation of the bearing profiles during hot conditions.
- The main bearing edge loading shows similar levels of asperity contact pressure both for sprayed and non-sprayed bearing supports.
- Inside the lower main bearing shell in the middle region, sprayed bearing supports show locally higher asperity contact pressure compared to non-sprayed. However, larger areas with high levels are shown in the case of non-spray.
- The sprayed bearing supports generally show about 20 % less asperity friction loss compared to non-sprayed bearing supports meaning that there are higher thermal load without spray.
- Non-sprayed bearing supports also increase the risk for cracks in bedplate.
- Overall, sprayed bearing supports are recommended regarding friction loss, fuel consumption and bedplate durability. Regarding main bearing performance the results are more or less equal between the two cases.

1.2 Purpose and goal

The conclusions drawn from the earlier work lead to a recommendation of investigating other designs of the main bearing supports that could replace the sprayed supports with the same or better performance. If such a design would be found without having to use spray, or alternatively less spray, it could be a significant saving cost for VCC.

1.3 Delimitations

The project does not not use parametric design of the main bearing supports to find an optimum design with regards to functionality. Such a project would need to consider not only scope of the functionality of the main bearing supports, but would also have to consider manufacturing capability and the cost to do so as such. Other aspects to consider in such a case would also be noise, vibration and harshness. No more than four different main bearing support designs will be evaluated. These designs are based on ideas and discussion among design engineers and CAE-engineers at VCC.

1.4 Objective

The main objective is to evaluate and compare four different design proposals of main bearing supports without spray with sprayed bearing supports, in order to evaluate whether the designs can replace the sprayed bearing supports or not. This will be done by simulating different designs of bearing supports without spray and compare to the current design with spray regarding:

- Deformed main bearing profiles.
- Contact behaviour between the bedplate and main bearing supports during hot conditions.
- Total pressure and asperity contact pressure for each main bearing.
- Friction loss in all main bearings.

2

Theory

2.1 Main Bearings

In the VEA-engines, as in most automobile engines, plain bearings are used for the main bearings to the crankshaft. In order to assemble the main bearings around the crankshaft the bearings are divided into two halves, a top and a bottom shell. A picture of two main bearing halves can be seen in Figure 2.2. The main bearings are assembled between each cylinder and since all VEA-engines have four cylinders there are five main bearings on the crankshaft. The top shell of each main bearing has an oil groove and three oil holes for the supply and smooth distribution of lubrication oil. On the crankshaft there are also two lubrication bores which pass main bearing #2 and #4. These lubrication bores are there to supply the rod bearings with lubrication oil which comes via the lubrication holes of main bearing, MB, #2 and #4. The numbering of the main bearings are shown in Figure 2.1. Main bearing #4 can also handle axial forces besides radial forces from the crankshaft [4]. The bottom bearing shell has three layers of different materials which are shown in Table 2.1.

Material	**Layer thickness [mm]**	E **[GPa]**	**Hardness**
Wismut (Bi)	0.005	32	HB: 70-95 MPa Mohs: 2-2.5
Silver (Ag)	0.004	76	HV: 206-250 MPa HB: 250 MPa
Aluminium alloy	0.3	N.A	HV5: 90
Steel	1.7	210	HV10: 220

Table 2.1: Bearing data for the the main bearings used in the VEA-engines [5].

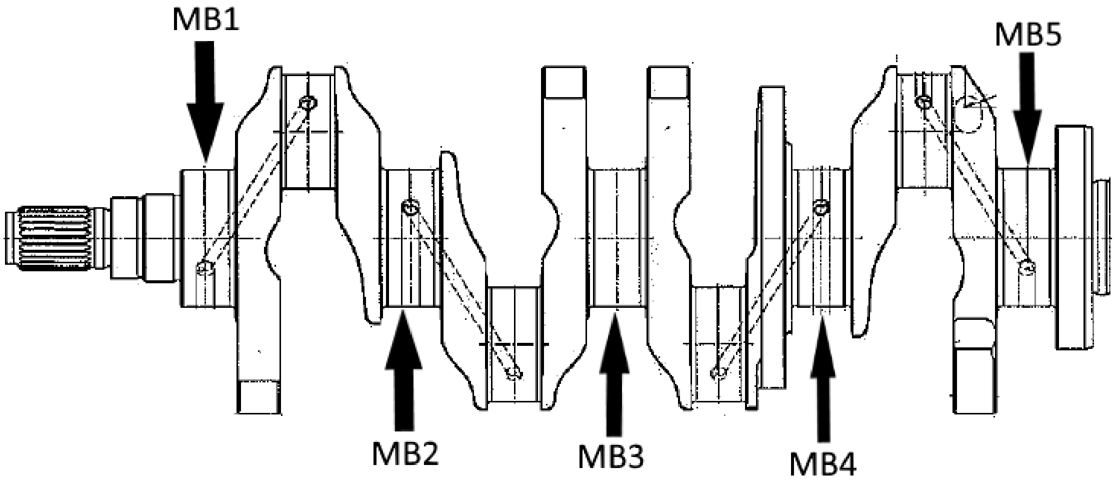

Figure 2.1: Drawing of a crankshaft used in older generations of VEA-engines. The location of the main bearings are displayed in the figure with arrows marking their locations on the crankshaft. As shown in the drawing, the supply paths of lubrication oil, the dotted lines, are between each MB and rod bearing which is not the case in the new generation of VEA-engines. In the newer engines MB2 and MB4 supply their adjacent rod bearings with lubrication oil.

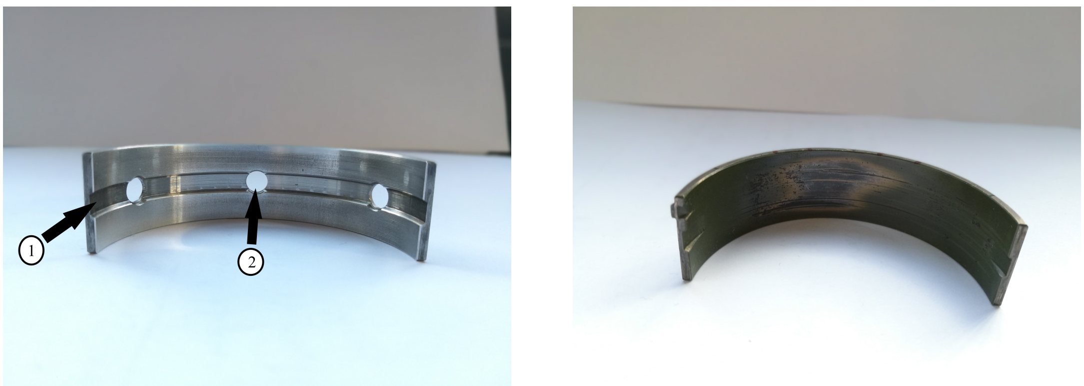

(a) (b)

Figure 2.2: Two halves of used plain bearings, the top half is shown to the left, (a), while the bottom half is shown to the right, (b). Lubrication hole 2 and lubrication groove 1 is shown in (a).

2.1.1 Lubrication

In automotive combustion engines, journal bearings are exposed to a variety of different conditions in terms of loads, speeds and temperatures. Following the Stribeck-curve shown in Figure 2.3, the friction coefficient may range depending on relative speed, load and lubricant viscosity from purely hydrodynamic lubrication with a sufficiently thick oil film to mixed or even boundary lubrication with significant amounts of asperity contact [6]. The lubricating oil flows in the grooves and travels in the direction of rotation by adhering to the surface of the crankshaft. In conjunction with the lubricating wedge formed by the shaft's eccentric shift relative to the bearing, the produced drag flow builds up pressure in the lubricating oil. The pressure field produced acts as a spring force. In addition to its rotary motion, the load causes the shaft to execute movements with a radial component. This squeezes the lubricant out of the decreasing lubricating gap in both circumferential directions and in both axial directions. The pressure field this process produces acts as a damping force. The pressure fields from rotation and displacement superimpose on each other, thus producing a pressure field that generates the bearing reaction force that separates the sliding surfaces of the shaft and bearing. Figure 2.4 presents the two pressure fields and the related bearing reaction forces [7].

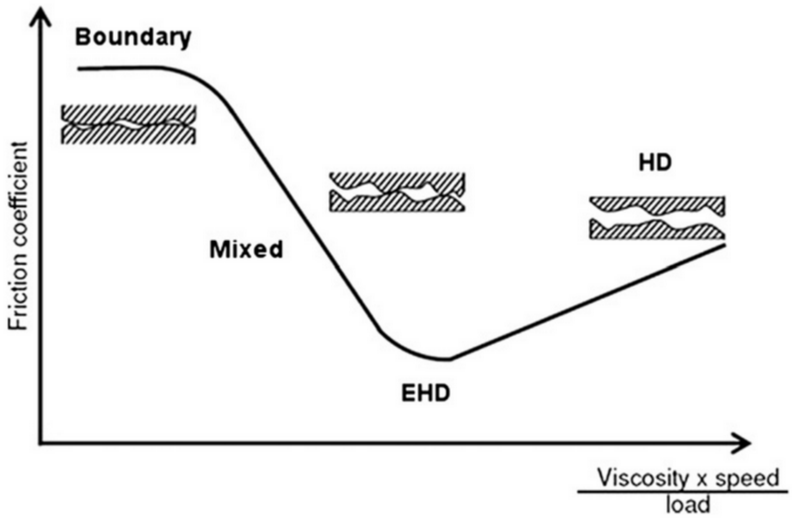

Figure 2.3: The different phases of lubrication according to Stribeck: Hydrodynamic (HD), elastohydrodynamic (EHD), mixed and boundary lubrication. The figure is taken from [6].

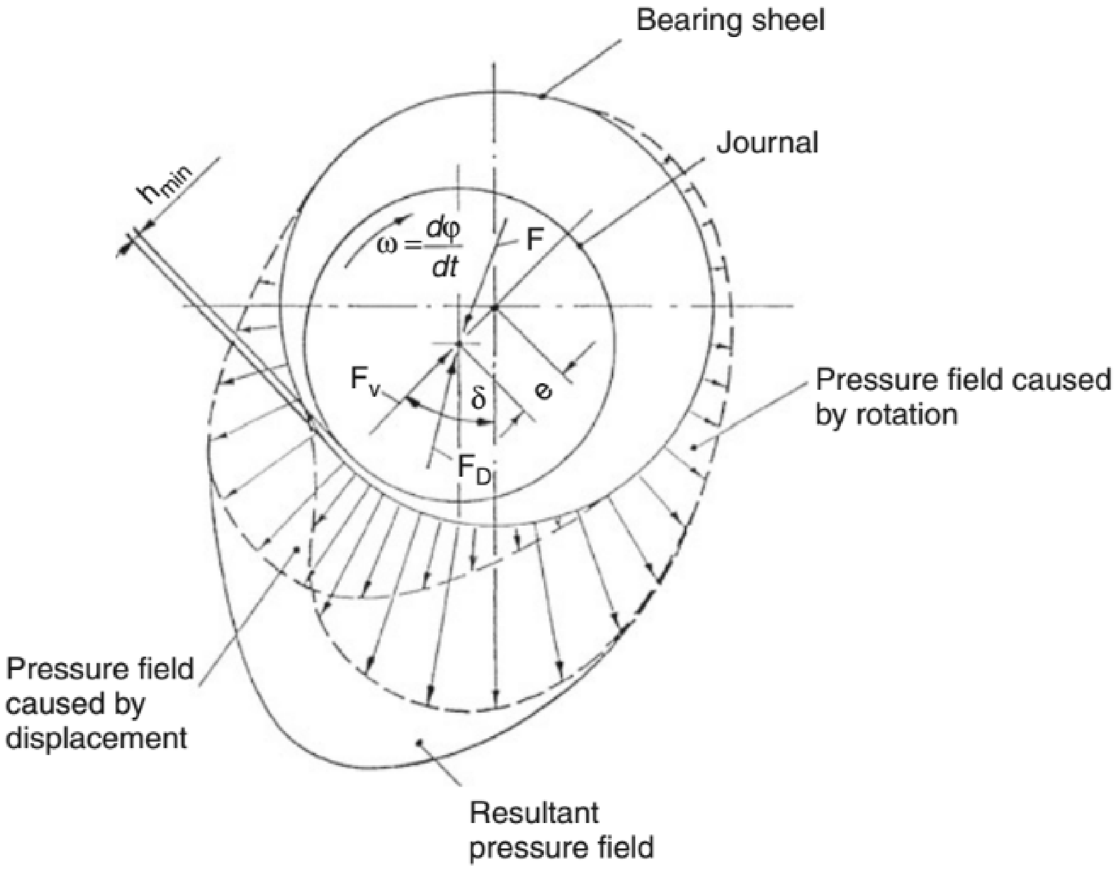

Figure 2.4: Pressure buildup in the lubricant of loaded hydrodynamic plain bearing. Here F is the bearing load force, F_{d} is the bearing reaction force from the pressure field due to rotation, F_v is the bearing reaction force from the pressure field due to displacement, e is the journal eccentricity, δ is the position angle of journal eccentricity, h_{min} is the minimum lubricating film thickness and ω is the angular velocity of the journal. The figure is taken from [7].

2.1.1.1 Boundary Lubrication

For boundary lubrication operating condition the pressure of the oil film is negligible and asperity contact between the two sliding surfaces occur. These are the most severe condition for any bearing as it is characterised by high friction and high wear. From a lubrication point of view the surfaces are at best partially inhibited from direct metal to metal contact due to boundary layers formed by friction reducing additives contained in the engine oil and a small amount of oil which is wetting the surfaces [7].

2.1.1.2 Mixed Lubrication

Mixed Lubrication is characterised by the simultaneous presence of boundary and hydrodynamic lubrication. Due to the small lubricating gap single asperities of both sliding surfaces are in contact with each other and break the oil film, with the consequence that no coherent oil film is present [7].

2.1.1.3 Hydrodynamic operation

For numerical simulation of bearing loads there can be numerous idealised assumptions made. One such assumption is that the bearing geometry is completely rigid. In earlier engines, lower loads and sizing provided with reserves made this a reasonable assumption. But with enhanced performance of engines and lightweight construction, specific bearing loads now produce such large deformations that they must be taken into account for the mathematical model to be more reliable [7].

2.1.1.4 Elasto-hydrodynamic operation

Elasto-hydrodynamic operation incorporates mechanical-elastic component deformations unlike HD. The excitation forces are computed from hydrodynamic pressure and hydrodynamic friction via integration. The hydrodynamic pressure distribution of the oil film in a lubrication region between two bodies can be calculated using a modified Reynolds equation derived from the Navier-Stokes equation and the equation of continuity [9], [10] and [11]. Depending on the application, both a simulation with elasto-hydrodynamics and without hydrodynamics consideration of the structural dynamics of the connected bodies can be performed. For the calculation of the hydrodynamic pressure in a clearance gap of a bearing some basic assumptions, as well as some simplifications can be made:

- laminar conditions and Newton fluid properties are assumed.
- stress terms dominate mass terms in the Navier – Stokes equation.
- Geometrically based assumptions due to the small clearance gap height dimension.
- Stoke's stick criterion is applied at the connected bodies surfaces,
- Introduction of a fill ratio for the consideration of mass conservation and
- transformation into a shell body fixed coordinate system in order to be able to use a time invariant calculation grid.

With the mentioned basic assumptions, Reynolds equation can be written as follows.

$$\begin{aligned} &-\frac{\partial}{\partial x}(\theta \cdot \varphi_{\mathrm{x}} \cdot \frac{h^3}{12\eta} \cdot \frac{\partial p}{\partial x}) - \frac{\partial}{\partial z}(\theta \cdot \varphi_{\mathrm{z}} \cdot \frac{h^3}{12\eta} \cdot \frac{\partial p}{\partial z}) \\ &+\frac{u_{\mathrm{journal}} - u_{\mathrm{shell}}}{2} \cdot \frac{\partial(\theta \cdot (\bar{h}_{\mathrm{T}} + \sigma \cdot \varphi_{\mathrm{s}}))}{\partial x} + \frac{\partial(\theta \cdot \bar{h}_{\mathrm{T}})}{\partial t} = 0 \end{aligned} \tag{2.1}$$

where the variables are

- $h_{\mathrm{T}}(x, z, t)$ is the total clearance gap height between the surfaces of the shell and journal,
- $h(x, z, t)$ is the nominal clearance gap height between the surfaces of the shell and journal,
- $\bar{h}_{\mathrm{T}}(x, z, t)$ is the the average clearance gap height between the surfaces of shell and journal,
- $\theta(x, z, t)$ is the oil percentage gap between the surfaces the shell and journal,
- $p(x, z, t)$ is the hydrodynamic pressure in the lubricant oil,
- $\eta(x, z, t)$ is the dynamic lubricant oil viscosity,
- $\varphi_{\mathrm{s}}(x, z)$ is the shear flow factor of the lubricant oil,

- $\varphi(x,z)$ is the pressure flow factor of the lubricant oil,
- σ is the deviation of summit height of the surfaces of the shell and journal and
- x is the circumferential coordinate

The averaged Reynolds equation is solved with respect to the hydrodynamic pressure $p(x,z,t)$ in regions where the gap is completely filled with oil, $\theta = 1$. A constant cavitation pressure p_c is assumed in cavitation regions and the averages Reynolds equation is solved there with respect to the oil fill ration $\theta(x,z,t)$. $\eta(x,z,t)$ is the dynamic lubricant viscosity, which may depend on the lubricant's pressure as well on its temperature and shear rate [8].

The total clearance gap height between the surfaces of the shell and journal is illustrated in Figure 2.5 and can be expressed as

$$h_\mathrm{T} = h + \delta_1 + \delta_2 \tag{2.2}$$

where h is the nominal clearance gap, δ_1 is the roughness amplitude of one of the two rotating bodies and δ_2 is the roughness amplitude of the other rotating body. The composite roughness value, σ, can be computed from the standard deviation of the clearance height of the two sliding surfaces σ_1 and σ_2

$$\sigma = \sqrt{\sigma_1^2 + \sigma_2^2} \tag{2.3}$$

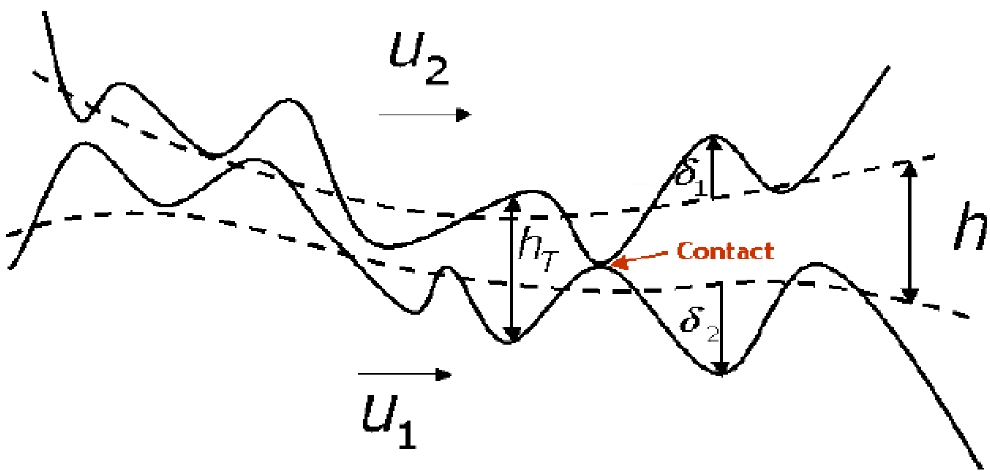

Figure 2.5: The figure shows two rotating bodies where u_1 and u_2 are components of the circumferential velocity of the two bodies respectively. The figure also show the total clearance gap height $h_\mathrm{T}(x,z,t)$, the nominal clearance height h and the roughness amplitude of the two bodies δ_1 and δ_2 respectively, are also shown. The figure is taken from [12]

.

2.1.1.5 Dry conditions

The nominal contact pressure P_a can, assuming a Gaussian distribution for the surface roughness and constant radius of the curvature for the asperity summits, be determined according to (derived by Greenwood and Tripp) [13].

$$P_{\mathrm{a}} = K \cdot E^{*} \cdot F_{5/2}(H_{\mathrm{s}}) \tag{2.4}$$

where K is the elastic factor, E^{*} is the elastic modulus and $F_{5/2}(H_{\mathrm{s}})$ is the form function. The elastic modulus, E^{*}, can be computed as

$$E^{*} = \frac{E_1}{1-\nu_1^2} + \frac{E_2}{(1-\nu_2^2)} \tag{2.5}$$

where E_1 is the Young's modulus and ν_1 is Poisson's ratio for one of the rotating bodies while E_2 is the Young's modulus and ν_2 is the Poisson's ratio for the other rotating body. The form function, $F_{5/2}(H_{\mathrm{s}})$, can be computed as

$$F_{5/2}(H_{\mathrm{s}}) = \begin{cases} 4.4086 \times 10^{-5}(4-H_{\mathrm{s}})^{6.804} \; for \; H_{\mathrm{s}} < 4 \\ 0 \; for \; H_{\mathrm{s}} \geq 4. \end{cases} \tag{2.6}$$

where H_{s} is the dimensionless clearance parameter and can be computed as

$$H_{\mathrm{s}} = \frac{h}{\sigma_{\mathrm{s}}} \tag{2.7}$$

where h is the nominal clearance height between the surfaces of the shell and journal and σ_{s} is the asperity summit roughness, which can be computed as

$$\sigma_{\mathrm{s}} = \sqrt{\frac{1}{N_{\mathrm{s}}} \sum_{i=1}^{N_{\mathrm{s}}} \delta_s^2(x_{\mathrm{i}})} \tag{2.8}$$

The elastic factor K can be computed as

$$K = \frac{16\sqrt{2}\pi}{15}(\sigma_{\mathrm{s}}\bar{\beta}_{\mathrm{s}}\eta_s)^2 \sqrt{\frac{\sigma_{\mathrm{s}}}{\bar{\beta}_{\mathrm{s}}}} \tag{2.9}$$

where η_{s} is the summit density and $\bar{\beta}_{\mathrm{s}}$ is the mean summit radius. Typically the elastic factor is in the interval $0.0003 \leq K \leq 0.003$. The mean summit radius $\bar{\beta}_{\mathrm{s}}$ can be computed as

$$\bar{\beta}_s = \frac{1}{N_{\mathrm{s}}} \cdot \sum_{i=1}^{N_{\mathrm{s}}} r(x_{\mathrm{i}}) \tag{2.10}$$

2.1.2 Friction loss

The total normal force, N_{Tot}, are made up of two parts [13]

$$N_{\mathrm{Tot}} = N_{\mathrm{Hydro}} + N_{\mathrm{Bound}} \tag{2.11}$$

where N_{Bound} is the normal force due to dry contact conditions and N_{Hydro} is the normal dynamic force due to lubricant in the gaps between the rotating bodies. This split also applies for the total friction force F_{Tot}, which can be expressed as

$$F_{\mathrm{Tot}} = F_{\mathrm{Hydro}} + F_{\mathrm{Bound}} \tag{2.12}$$

where F_{Hydro} is the hydrodynamic force, which can be expressed as the sum of the shear force, F_{Shear}, and the pressure force, F_{Pressure}, from the lubricant. With this in mind, F_{Tot} can be expressed as

$$F_{\text{Tot}} = F_{\text{Pressure}} + F_{\text{Shear}} + F_{\text{Bound}} \tag{2.13}$$

which in its final form can be expressed as

$$\begin{aligned} F_{\text{Tot}} = &\int_{-B/2}^{B/2}\int_{\phi_1}^{\phi_2}(\frac{h}{2}\cdot\frac{\partial p}{\partial \phi})\mathrm{d}\phi\mathrm{d}z \\ &+\int_{-B/2}^{B/2}\int_{\phi_3}^{\phi_4}(\eta\cdot\frac{R}{h}\cdot(R\cdot\omega+\dot{e}\cdot\sin(\phi)-e\cdot\dot{\gamma}\cdot\cos(\phi)))\mathrm{d}\phi\mathrm{d}z \\ &+\mu_{\text{Bound}}\cdot P_{\text{a}}\cdot A_{\text{a}} \end{aligned} \tag{2.14}$$

where

- μ_{Bound} is the friction coefficient of the boundary,
- ω is the angular velocity of the rotating body,
- P_a is the asperity contact pressure,
- A_a is the asperity contact area,
- $\frac{\partial p}{\partial \phi}$ is the pressure gradient along the azimuth angle ϕ,
- R is the inner shell radius,
- (e,γ) are the polar coordinates of the shaft displacement within the shell
- and $(\dot{e},\dot{\gamma})$ are the time derivatives of the polar coordinates of the shaft displacement within the shell.

2.2 Main bearing supports

Most internal combustion engines use a short shirt skirt design of the cylinder block [14]. The crank shaft is placed between the cylinder block and the main bearing supports, which are bolted together. In the top left illustration of Figure 2.6 a typical design of a main bearing support, used in most conventional automobile engines, is shown. For some high performance or heavy duty engines, it is necessary to increase the stiffness of the crankcase due to the high forces from the pistons. This can be achieved by using extended main bearing supports as seen in the in the lower left or with an extended skirt of the cylinder block as seen in the lower right. For engines with V-shaped cylinder engine configuration, there is also a significant horizontal component of the firing forces and so it might be necessary to angle the bolts as seen in the top right Figure 2.6.

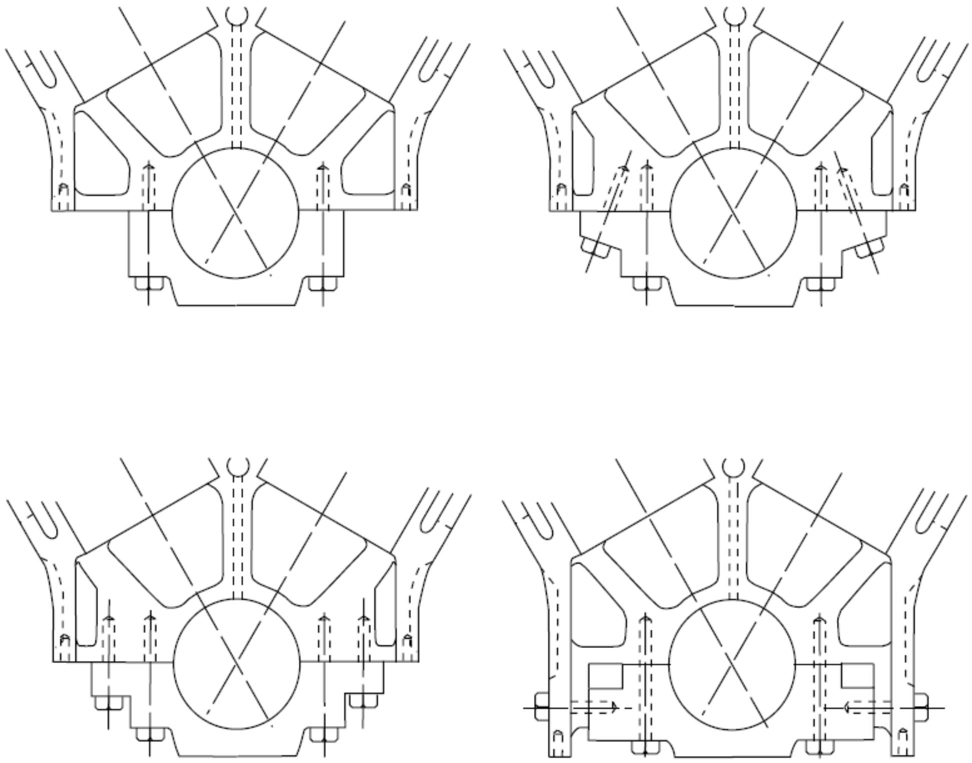

Figure 2.6: Illustrations of different types main bearing supports. Seen from top left to bottom right: A typical design of main bearing support utilising two bolts, extended main bearing support utilising four bolts, two of which are angled, are in V-shaped cylinder engine configuration. Four bolted main bearing supports are shown in the bottom right and bottom left, used for heavy performance and heavy duty engines respectively. The figure is taken from [14].

2.3 Spraying the main bearing supports

The main bearing supports, as mentioned earlier, are made of nodular iron. To improve the bonding between the bedplate and the main bearing supports they are sprayed with a thin layer of an aluminium alloy, AlSi12. A chemical bonding between the bedplate and the sprayed main bearing supports are achieved due to the fact that the aluminium coating partially re-melt when the aluminium melt of the bedplate hit the aluminium coating. This fuses the aluminium coated main bearing supports with the bedplate. The bonding provides a tight fit between the main bearing supports and the bedplate, which is important in order to prevent fatigue in the bedplate and for the deformation of the crank bore during running engine conditions [15].

3

Methods

The methodology is largely based on the work from [3], to make the results comparable with that of the sprayed bearing supports. The engine model used for all the analyses was a Volvo Engine Diesel 4 cylinder High Performance, VED4 HP.

3.1 Software

A number of software was used to perform the analyses.

- *ANSA v.16.1.0* [16] was used for pre-processing.
- *ABAQUS v.6.14-3* [17] was used for statical analyses producing deformed radial profiles of the main bearings.
- *ABAQUS viewer v.6.14-3* [18] was used to analyse the bonding between the bedplate and the main bearing supports.
- *MSC-Nastran*[19] was used to condense the model of the fully dressed engine.
- *AVL EXCITE PU v.2013.2* [20] was used for dynamic analyses to analyse pressure on the main bearings and the friction losses at certain engine speeds of the main bearings.
- *MATLAB 2015b* [21] was used for post processing.

The first three analyses in *ABAQUS* involved non-linear analyses of the cylinderblock, bedplate and main bearing supports. From the analyses the deformed profiles of the main bearings and the contact behaviour between the bedplate and the main bearings were extracted and used in the *AVL EXCITE PU* analyses.

3.2 Design proposals

Four design proposals were suggested [22], all are based on the current design, see Figure 3.1. Each of the design proposals were presented with the aim of providing a sufficient mechanical bonding with the bedplate.

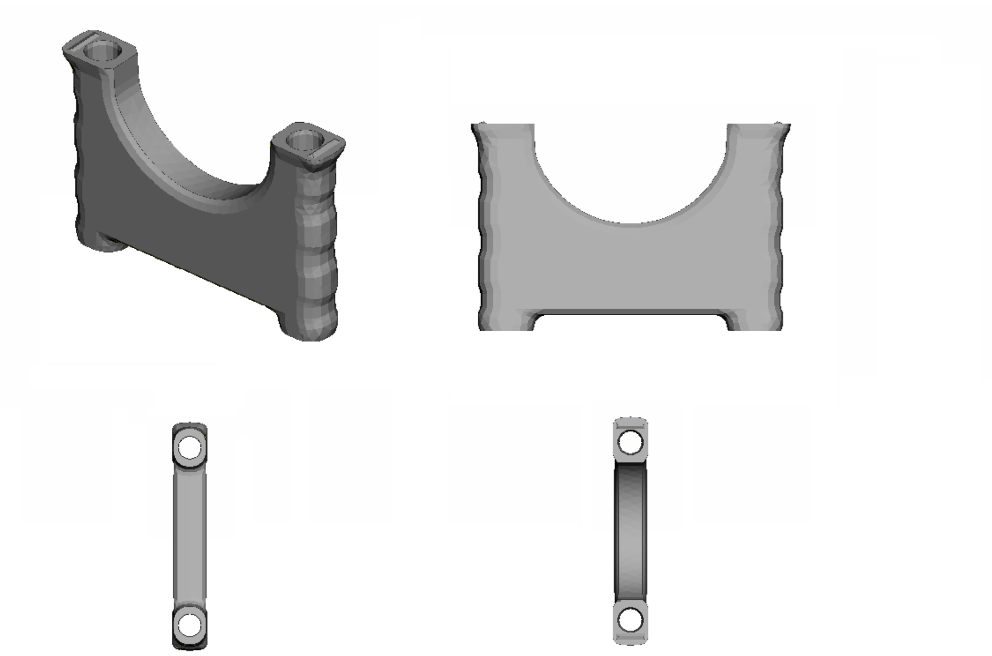

Figure 3.1: A CAD-model of the original main bearing support with sprayed coating displayed in different views. Displayed from top left to bottom right isometric view, front view, bottom view and top view.

3.2.1 #1 Al-pillar

The *Al-pillar* design is based on a current design in use in engines with a lower performance in the VEA-family. It has an oval shaped hole going through the center of the main bearing support, see Figure 3.2. When the bedplate is casted, melt from the aluminium alloy fills the hole in the center of the main bearing support. The pillar, created when the melt of the bedplate cools down, provides greater bonding between the bedplate and the main bearing support.

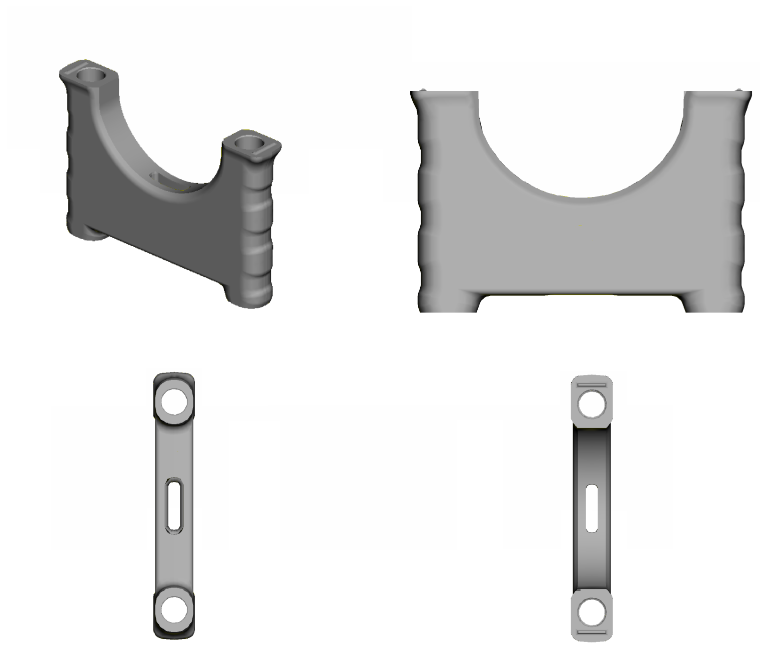

Figure 3.2: A CAD-model of the design proposal *Al-pillar*. Displayed from top left to bottom right: isometric view, front view, bottom view and top view

3.2.2 #2 Upper Groove

For the design *Upper Groove* a groove was inserted on the top face of the main bearing support, see Figure 3.3. The idea behind it was to observe what impact it would have on the bonding between the bedplate and the main bearing supports without having to make a hole through the structure.

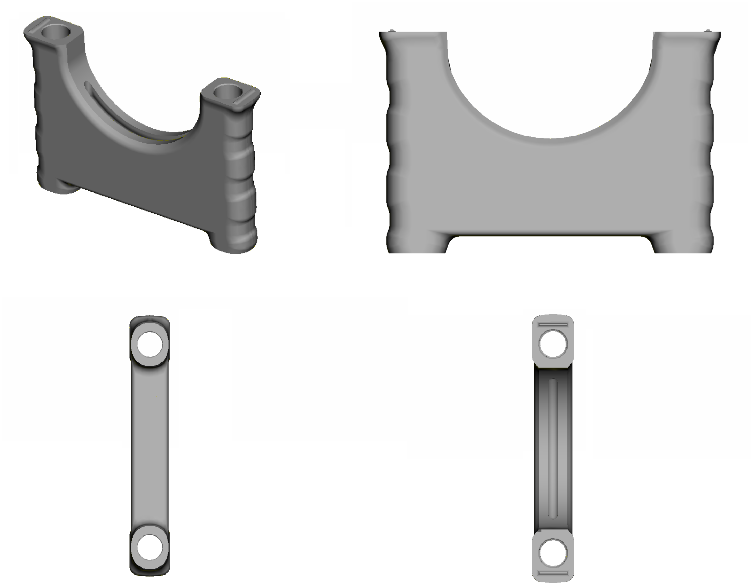

Figure 3.3: A CAD-model of the design proposal *Upper Groove*. Displayed from top left to bottom right: isometric view, front view, bottom view and top view

3.2.3 #3 Double Groove

The *Double Groove* design, as shown in Figure 3.4, has two grooves, one on the front face and one on the back face of the main bearing support. From [3] it could be observed that there was little bonding between the bedplate and the non-sprayed main bearing support. With a groove on the front and back face of the main bearing support it was believed that this problem would be remedied.

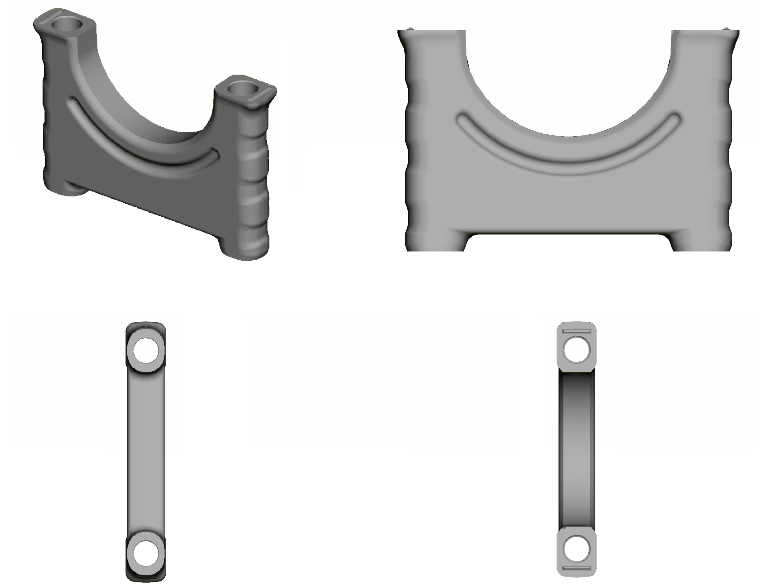

Figure 3.4: A CAD-model of the design proposal *Double Groove*. Displayed from top left to bottom right: isometric view, front view, bottom view and top view

3.2.4 #4 Combination of Grooves

Design proposal #4 is a combination of the design proposals #2 and #3 utilising a groove on the top face, the front face and the back faces, see Figure 3.5. This design inherits the strengths and weaknesses of both *Double Groove* and *Upper Groove*.

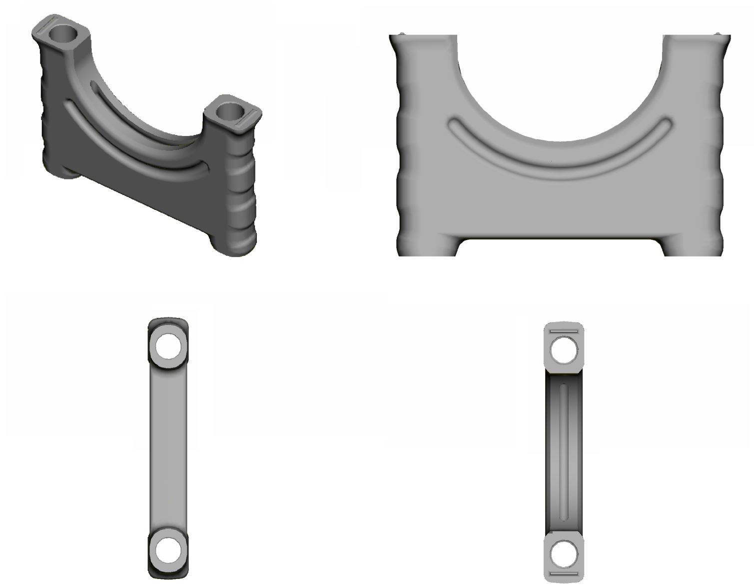

Figure 3.5: A CAD model of the design proposal *Combination of Grooves*. Displayed from top left to bottom right: isometric view, front view, bottom view and top view

3.3 Main bearing profiles and bonding between the bedplate and the main bearing supports

Each of the design proposals of the main bearing support were used in a model with parts of the base engine, as shown in Figure 3.6, in *ABAQUS*. Three static analyses were carried out in *ABAQUS*. Each of the analyses was performed to evaluate the bonding between the bedplate and the main bearing supports and also to extract the radial deformations of the profiles of the main bearings. The final analysis was made to check that the bonding between the bedplate and the main bearing supports had not changed significantly. The analyses were conducted in the following order:

1. Residual stresses from casting and machining
   - 1.1. Cooling down from 200 °C to 20 °C
   - 1.2. Machining operations. Removing parts belonging to the cylinder block and bedplate from manufacturing.
2. Pretentions of bolts
   - 2.1. Pretention of bolts (bedplate to cylinderblock).
   - 2.2. Shrink fit of main bearings
   - 2.3. Thermal expansion from 20 °C to 130 °C
3. Main bearing forces from the crank shaft
   - 3.1. Max loading at main bearing #1
   - 3.2. Max loading on main bearing #2
   - 3.3. Max loading on main bearing #3
   - 3.4. Max loading on main bearing #4
   - 3.5. Max loading on main bearing #5
   - 3.6. Max loading on main bearing #3

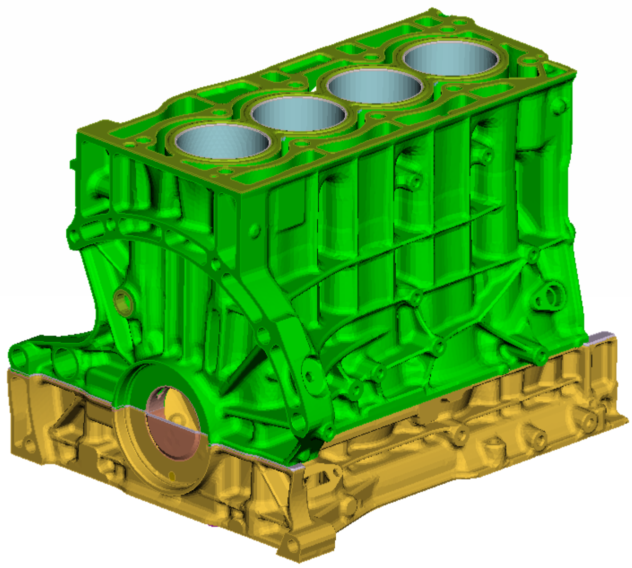

Figure 3.6: A CAD model of the base engine which included the cylinder block, bedplate and the main bearing supports. The model was used for the static analyses in *ABAQUS*. The green structure represents the cylinder block and the dark yellow structure represents the bedplate.

3.3.1 Mesh quality criterion

For the volume mesh of the main bearing supports, a number of mesh quality criterion was used which are standard in the *Engine CAE* department at VCC for this type of analyses. The mesh quality criterion are presented in Table 3.1.

Element type	Tetrahedral second order
Element length	2-6 mm
Aspect ratio	8
Jacobian	0.7
Min angle trias	5
Max angle trias	175
Mid point deviation	6 %
Mid point alignment	10 %
Skewness	0.5

Table 3.1: The mesh quality criterion used for the main bearing supports in the analyses for the static analyses in *ABAQUS*.

3.3.1.1 Contact defintion

A contact definition between the bedplate and the bearing supports was used for the static analyses. The surfaces in contact experienced finite sliding with the linear penalty method, which can be studied more in detail in [23]. A static friction coefficient of $\mu = 0.15$ was also included in the definition [3].

3.3.2 Post processing

3.3.2.1 Contact areas between the bedplate and main bearing supports

The surfaces of the main bearing supports, which were in contact with the bedplate, were "pasted" together. This prevented any relative motion between the surfaces, which were in contact. An important simplification was also made where surfaces of the main bearing supports, which where slipping on the bedplate, would be assumed to be sticking to the bedplate. For the sprayed main bearing supports, the outer surfaces of the main bearing supports were assumed to be sticking to the bedplate [3].

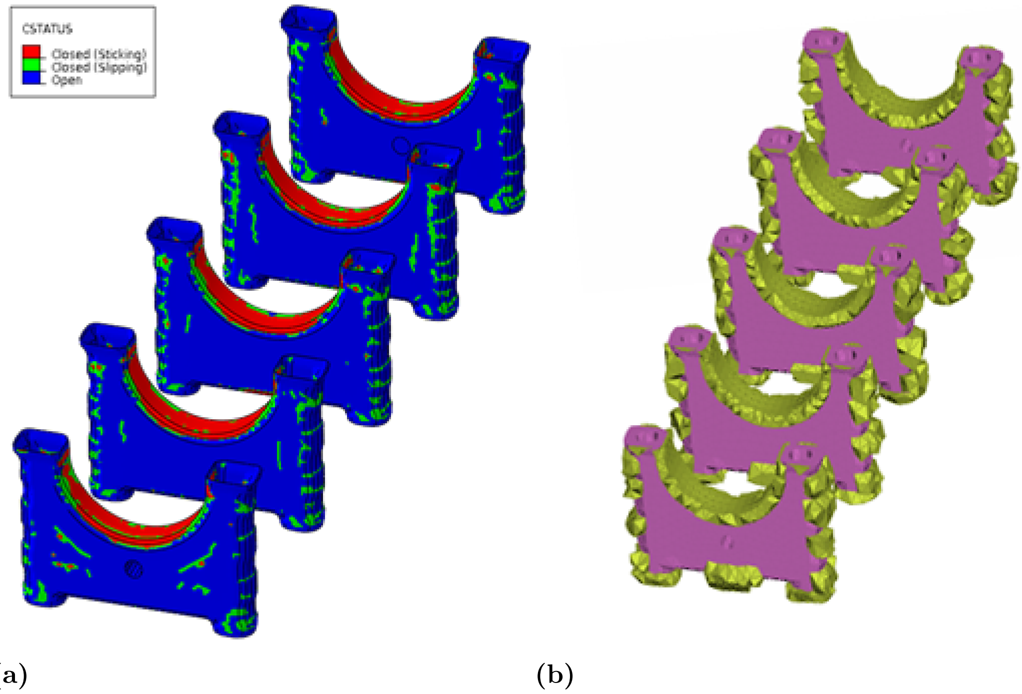

(a) (b)

Figure 3.7: Shown in the left figure, (a), is the contact status between the main bearing supports and the bedplate at 130 °C. The red areas indicate that the surfaces of the main bearing supports are sticking to the bedplate. The green areas indicate that the surfaces of the main bearing supports are slipping on the bedplate. The blue areas indicate that the surfaces of the main bearing supports and the bedplate are seperated. In the right figure, (b), the elements, in yellow, of the bedplate sticking to the main bearing supports according to the contact status is shown.

3.3.2.2 Main bearing profiles

In Figure 3.8 it can be observed how the degrees are measured on the two bearing halves of each main bearing. Beside the radial deformation of the main bearing profiles, due to the thermal load from the *ABAQUS* analyses, radial deformations to the main bearing profiles' edges were also added. The added edge deformations come from measurements from a physical test, where a VED4 HP was run for 500 hours with full load. The engine was run through a number of engine speeds, from 1000 rpm to 5000 rpm. The values of the radial edge deformation added to the main bearings can be seen in Table 3.2 [5]. An example of the deformed main bearing profiles due to the thermal load and with the added edge deformations, can be observed in Figure 3.9.

Upper half	7.0 μm
Lower half front end	7.0 μm
Lower half back end	10.0 μm

Table 3.2: Table showing the values of the added edge deformation to the main bearing profile.

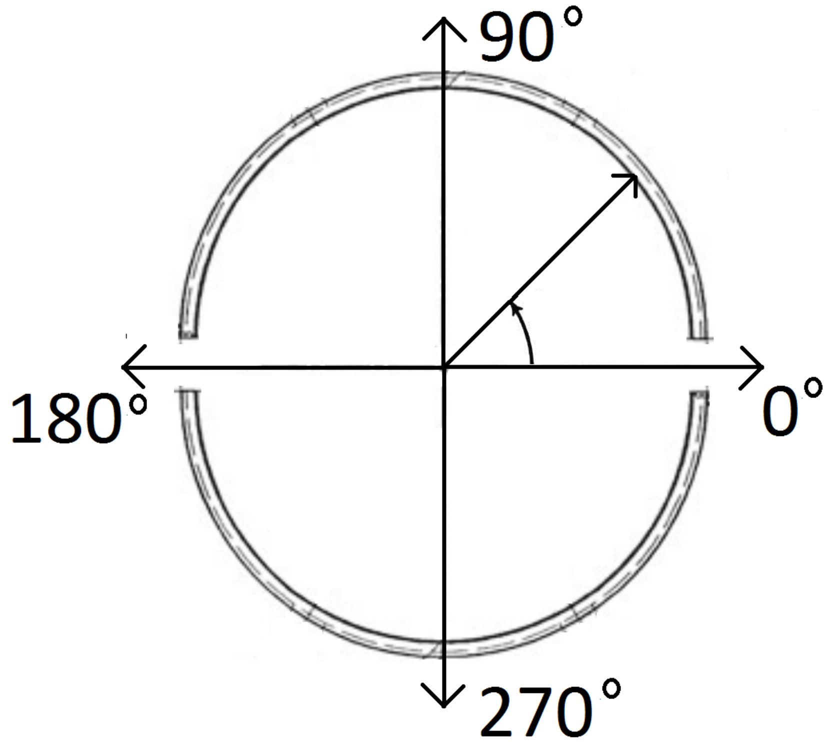

Figure 3.8: An illustration of the two bearing shell. 0° and 180° mark where the two bearing halves meet.

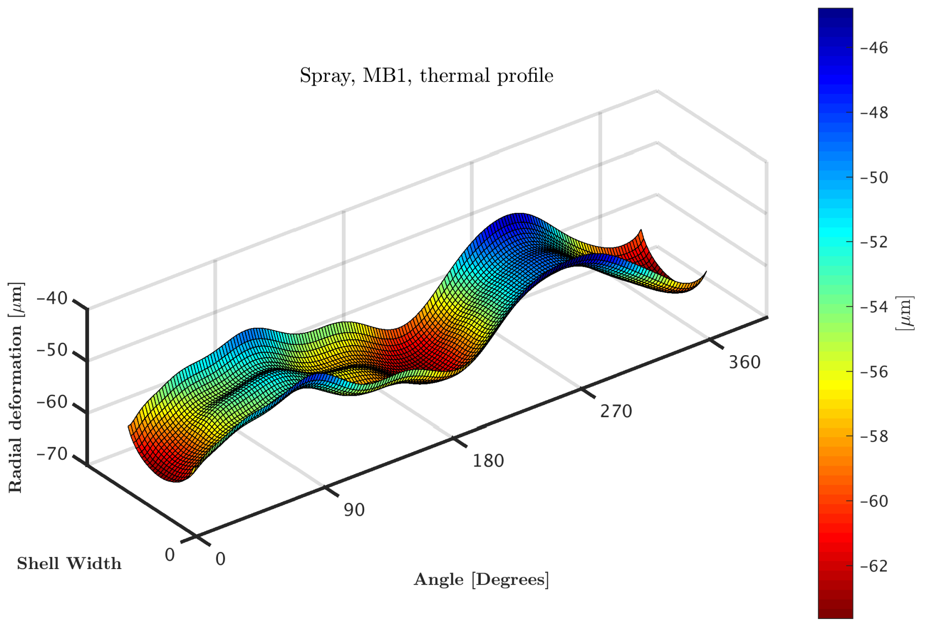

(a)

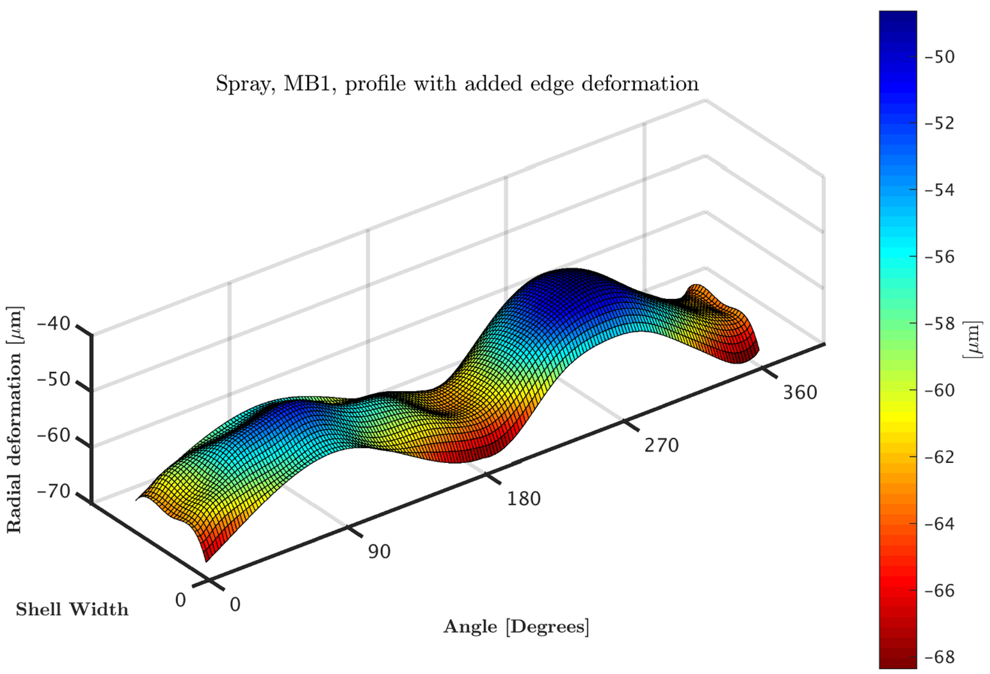

(b)

Figure 3.9: MB1 unwrapped with the radial deformations of the profile for a sprayed main bearing support, shown in (a) at 130 °C and shown in (b) with applied deformations to the edges.

3.4 AVL EXCITE PU

In *AVL EXCITE PU* a system of flexible bodies was used for the dynamic analyses. A fully dressed model of the engine was also used, see Figure 3.10, together with other substructures such as crankshaft, conrod, bearings etc. as can be observed in Figure 3.11. The degrees of freedom of so many structures become large and computationally expensive. A reduction of the degrees of freedom is therefore necessary and also a method of coupling the different substructures needs to be employed. The chosen method was CMS Craig-Bampton, which can be studied more in detail in [24]. It was chosen due to the favour of shorter computational time. The design proposals of the main bearing supports, with the contact behaviour according to the analyses made in *ABAQUS*, were imported to *AVL EXCITE PU*.

3.4.1 AVL EXCITE PU model

Table 3.3 show some of the settings used for the model in *AVL EXCITE PU*. Table 3.4 show some of the values for the parameters in the asperity contact model used in *AVL EXCITE PU*.

Engine	Diesel I4 231 hp
Number of engine cycles	4
Engine speeds	1000-5000 rpm; increment of 250 rpm
Friction coefficient	0.01
Oil quality	SAE 5W-20
Hydrodynamic Mesh	25 x 180
Lubrication model	EHD2 Mixed lubrication
Operating temperature	130 °C
Main Bearing Diameter	60 mm
Main Bearing Width	18.75 mm
Radial clearance	20 μm

Table 3.3: Table showing some of the input data used in *AVL EXCITE PU*.

Summit Roughness	0.001 mm
Young's Modulus	68 GPa
Elastic Factor	0.008

Table 3.4: Table showing the parameters and their values used for the asperity contact model in *AVL EXCITE PU*.

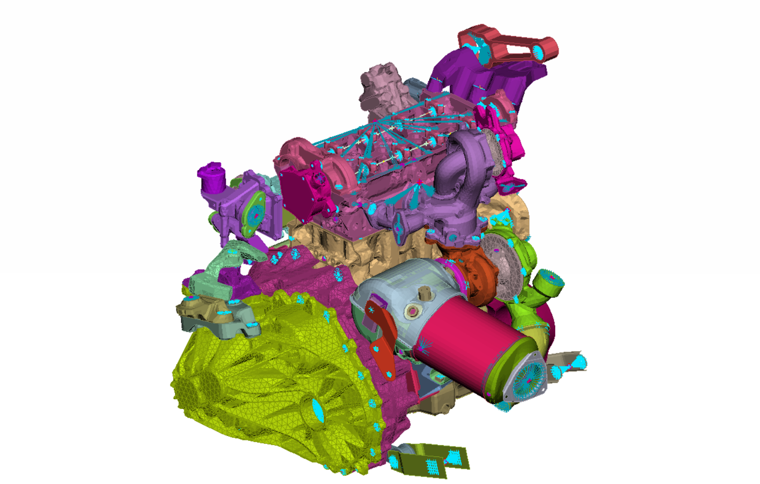

Figure 3.10: A CAD-model of the fully dressed engine, VED4 HP, used for the *AVL EXCITE PU* analysis

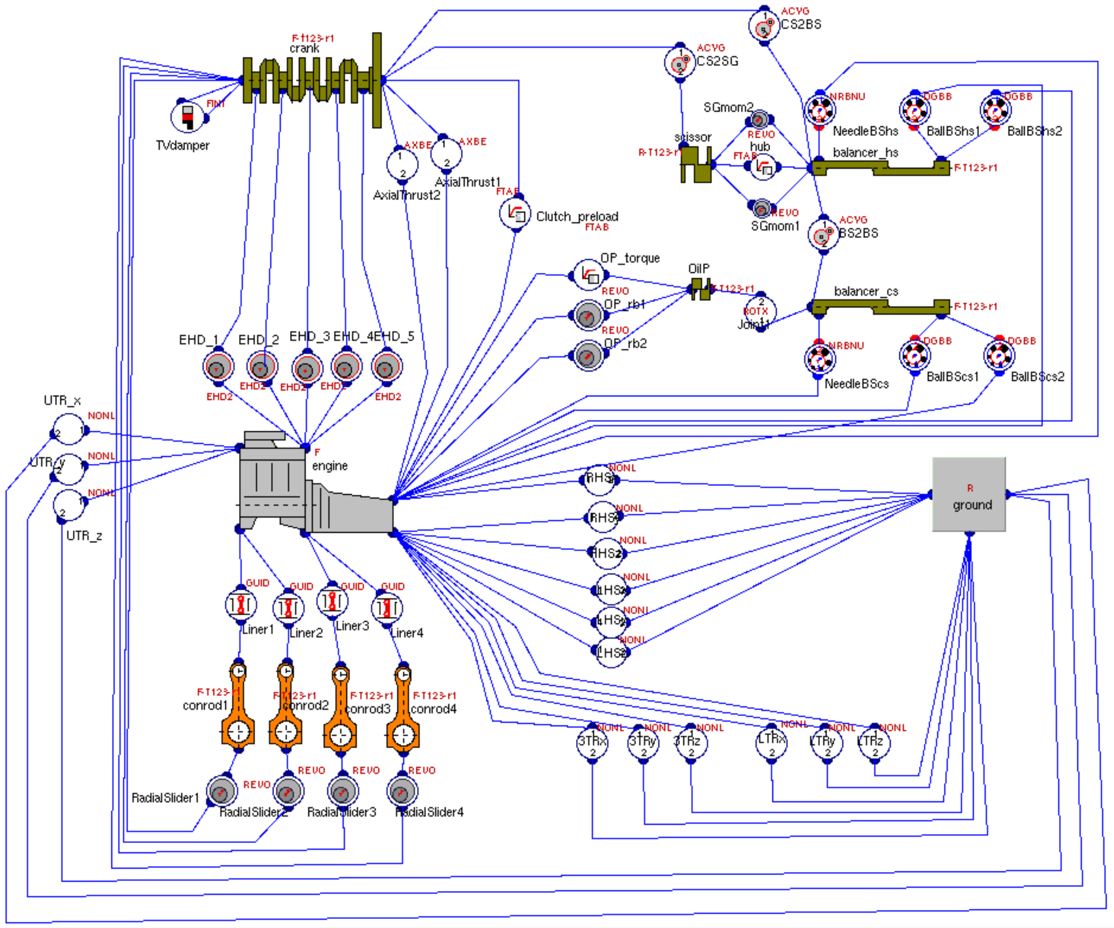

Figure 3.11: A 2D view of the different body components used in *AVL EXCITE PU* and their connections between different nodes.

3.4.2 Cylinder pressure and Engine torque

Each cylinder in the engine model used in *AVL EXCITE PU*, used the same pressure variation over an engine cycle to drive the pistons. The cylinder pressure varies with the position of the crank shaft, known as crankangle. Figure 3.12 show the cylinder pressure for three different engine speeds. A torque with the opposite direction of the torque produced by the engine, was also applied on the flywheel in the *AVL EXCITE PU* model, to keep a steady engine speed. The torque produced by the engine at the different crank angles is shown in Figure 3.12.

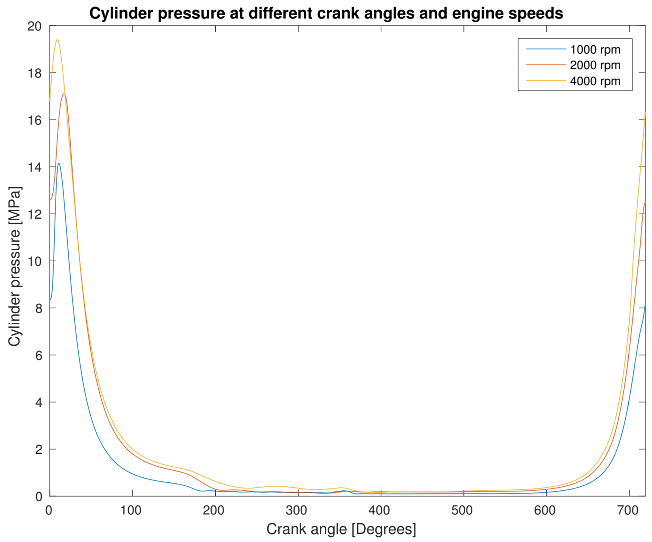

(a)

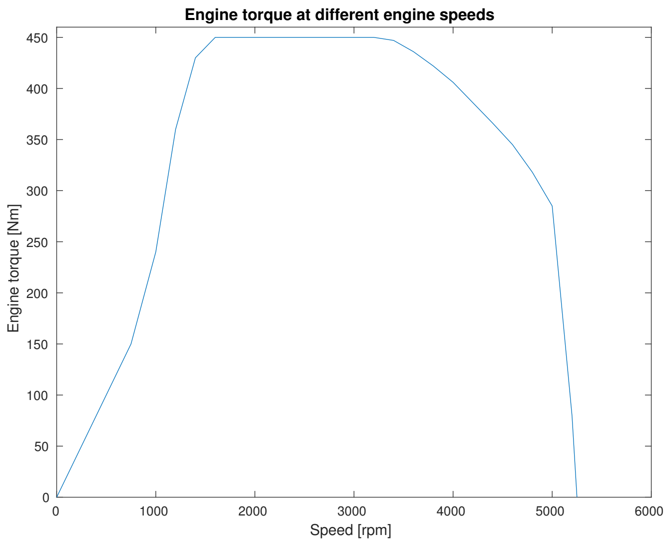

(b)

Figure 3.12: The cylinder pressure at different crank angles for different engine speeds shown in the top figure, (a). The engine torque at different crank angles produced is shown in the bottom figure, (b).

3.4.3 Post processing

The results extracted and analysed from *AVL EXCITE PU* were from the last two engine cycles. This was done because of transients appearing in in the first two engine cycles. The simulation needed time to stabilise before valid results could be obtained. The extracted data were then plotted and compared to the concept *Spray* using scripts written in *MATLAB*. In the case of investigating the risk of wear, it was of interest to investigate the asperity contact pressure and compare it for the different design proposals with the sprayed main bearing supports. For the friction loss of each bearing, it was primarily the total friction loss that was of interest.

4
Results

4.1 Deformed main bearing profiles

The deformed bearing profiles of each main bearing and design proposal with the applied edge deformation can be viewed in Appendix A.

4.2 Contact status between the bedplate and the main bearing supports

In this section the bonding between the bedplate and the main bearing supports at the engines operating temperature, i.e 130 °C, is presented for each design proposal. Surface plots of the main bearing supports are shown in figures and in different views to show where there is any contact with the bedplate.

4.2.1 Contact status for Al-pillar

In Figure 4.1 it can be observed that all the main bearing supports have similar surface areas, which are sticking to the bedplate or slipping on the bedplate. In the same figure it can be observed that most of the inner surface, where the pillar of the bedplate comes through, are sticking to the bedplate. Most of the top surfaces of the main bearing supports are sticking to the bedplate with the exception for main bearing support # 2 where a large part of the edges are slipping on the bedplate, as observed in Figure 4.2. In the same figure we can observe that the bottom surfaces, around the hole in the center, of the main bearing supports are sticking to the bedplate.

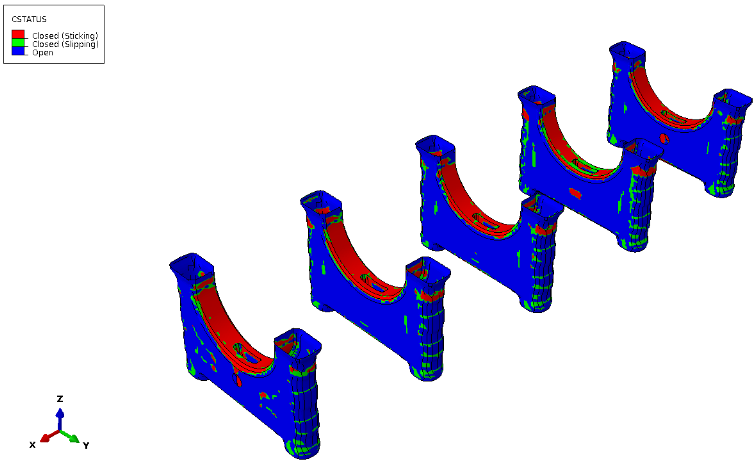

(a)

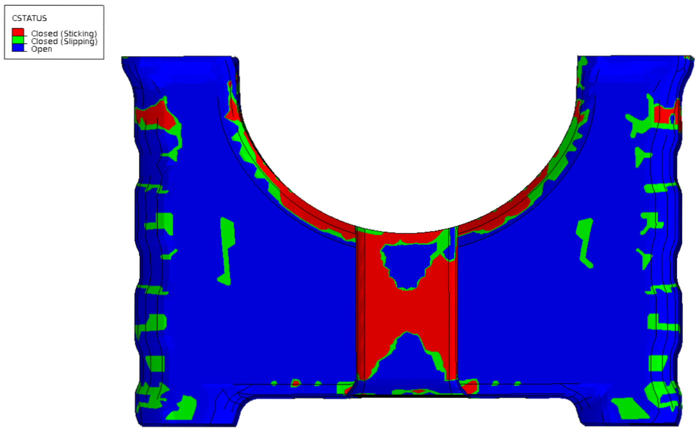

(b)

Figure 4.1: The top figure, (a), shows the contact status between the main bearing supports, with the *Al-pillar* design, while the bottom figure, (b), shows a cutsection view of the main bearing support #3. The red areas indicate that the surfaces of the main bearing support are sticking to the bedplate. The green areas indicate that the surfaces of the main bearing support are slipping on the bedplate. The blue areas indicate that the surfaces of the main bearing support and the bedplate are seperated.

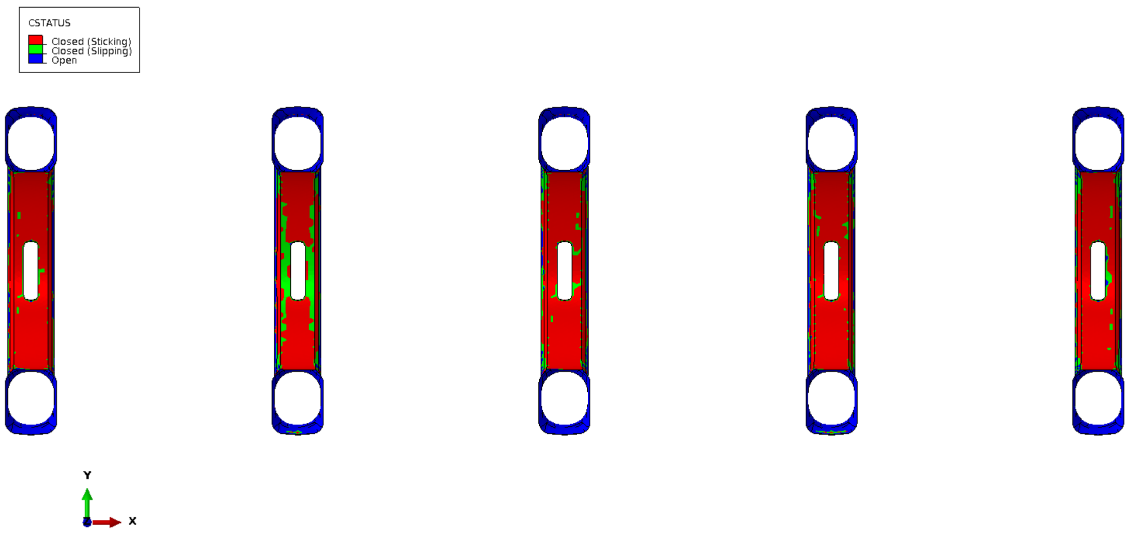

(a)

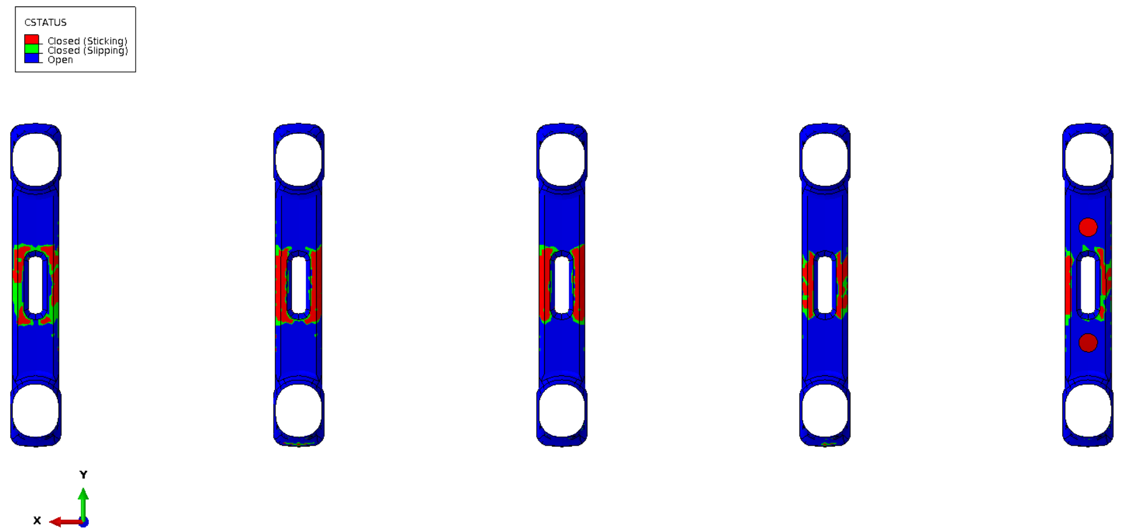

(b)

Figure 4.2: The top figure, (a), shows a top view of the contact status between the main bearing supports, with the *Al-pillar* design, while the bottom figure, (b), shows a bottom view of the contact status between the bedplate and the main bearing support. The red areas indicate that the surfaces of the main bearing supports are sticking to the bedplate. The green areas indicate that the surfaces of the main bearing supports are slipping on the bedplate. The blue areas indicate that the surfaces of the main bearing supports and the bedplate are seperated.

4.2.2 Upper Groove

In Figure 4.3 it can be observed that most of the bonding between the bedplate and the main bearing supports occur on the top surfaces, the sides and inside the groove on the top surface. Around the groove on the top surfaces of the main bearing supports there are, however, bonding with the bedplate, as observed in Figure 4.4. In the same figure, it can be observed that most of the bottom surfaces of the main bearing supports are not sticking to the bedplate, except for the middle at the edges and with an exception for main bearing support # 5.

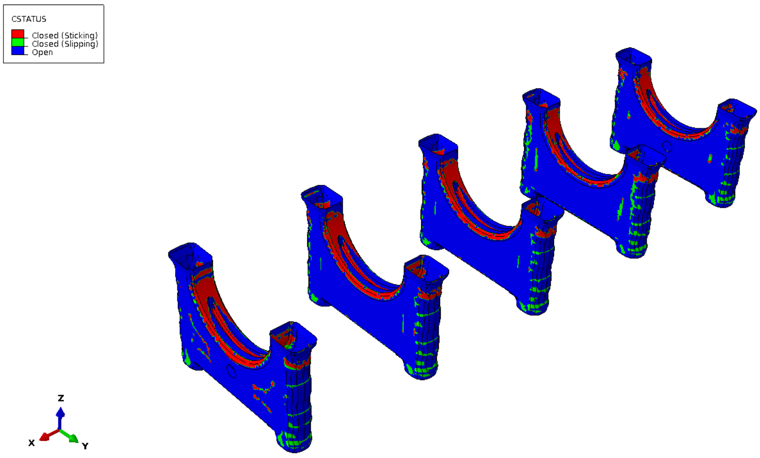

(a)

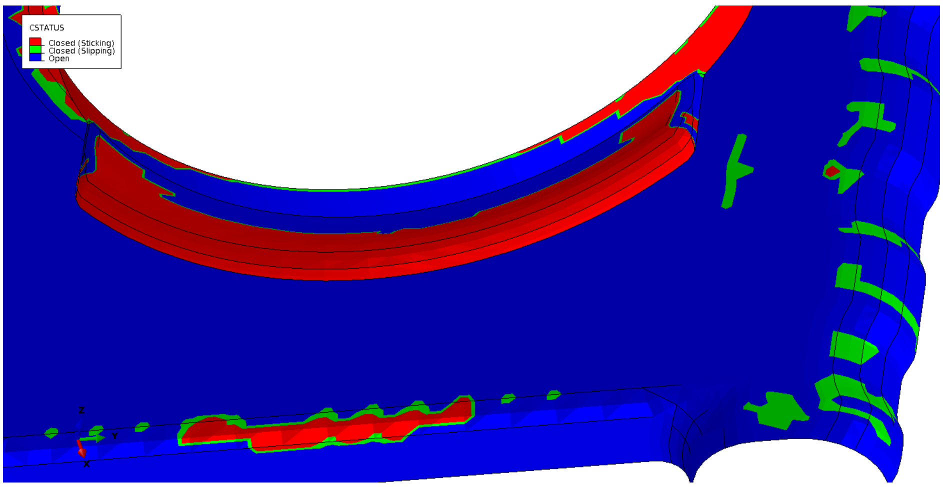

(b)

Figure 4.3: The top figure, (a), shows the contact status between the main bearing supports, with the *Upper Groove* design, while the bottom figure, (b), shows a cutsection view of the main bearing support #3. The red areas indicate that the surfaces of the main bearing supports are sticking to the bedplate. The green areas indicate that the surfaces of the main bearing supports are slipping on the bedplate. The blue areas indicate that the surfaces of the main bearing supports and the bedplate are seperated.

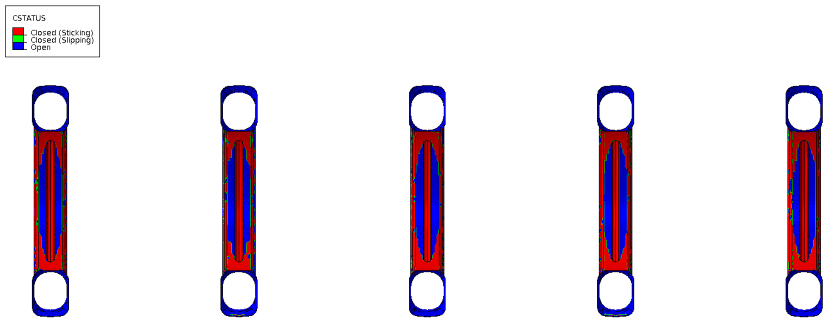

(a)

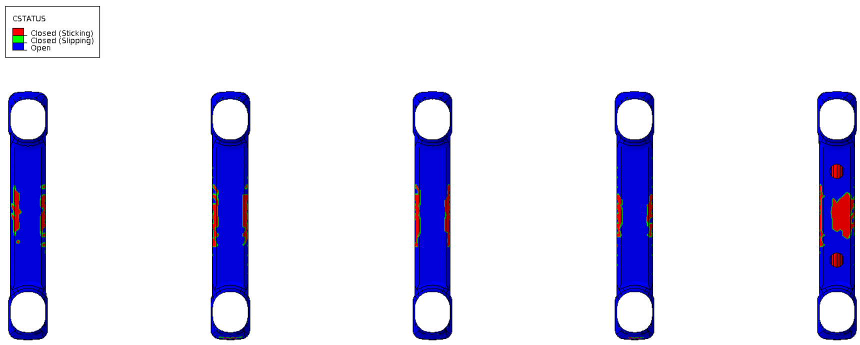

(b)

Figure 4.4: The top figure, (a), shows a top view of the contact status between the main bearing supports, with the *Upper Groove* design, while the bottom figure, (b), shows a bottom view of the contact status between the bedplate and the main bearing supports. The red areas indicate that the surfaces of the main bearing supports are sticking to the bedplate. The green areas indicate that the surfaces of the main bearing supports are slipping on the bedplate. The blue areas indicate that the surfaces of the main bearing supports and the bedplate are seperated.

4.2.3 Double Groove

In Figure 4.5 it can be observed that most of the surfaces bonding to the bedplate are the top surfaces and the sides. In the same figure, inside the groove on the front and back face, it can be observed that there are almost no surfaces that are in contact with the bedplate. Two thin lines in the grooves on each side are all that provide any bonding with the bedplate . In Figure 4.6, it can be observed that part of the edges of the top surfaces of the main bearing supports have no contact with the bedplate. But most of the surfaces on the top sides of the main bearing supports are in contact with the bedplate. Like the *Upper Groove*, there are small regions on the bottom surfaces of the main bearing supports, where the surfaces are sticking to the bedplate, which can be observed in Figure 4.6.

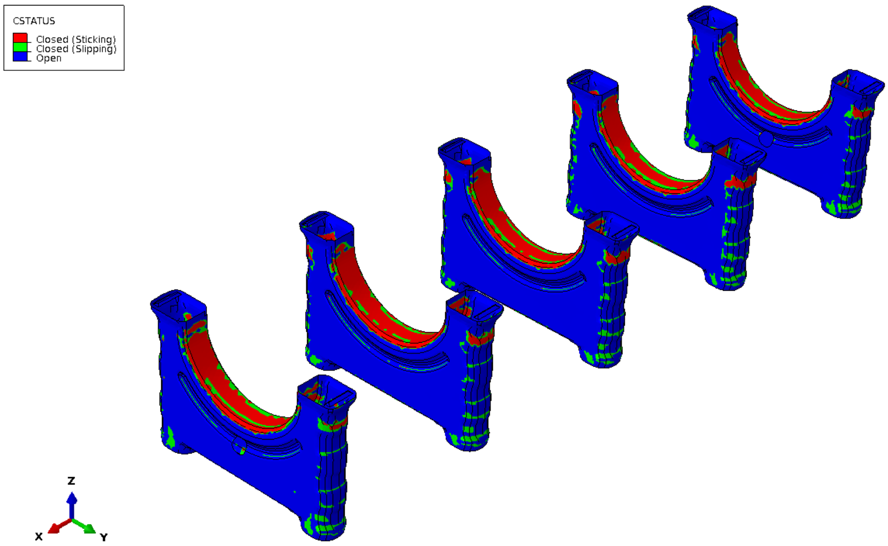

(a)

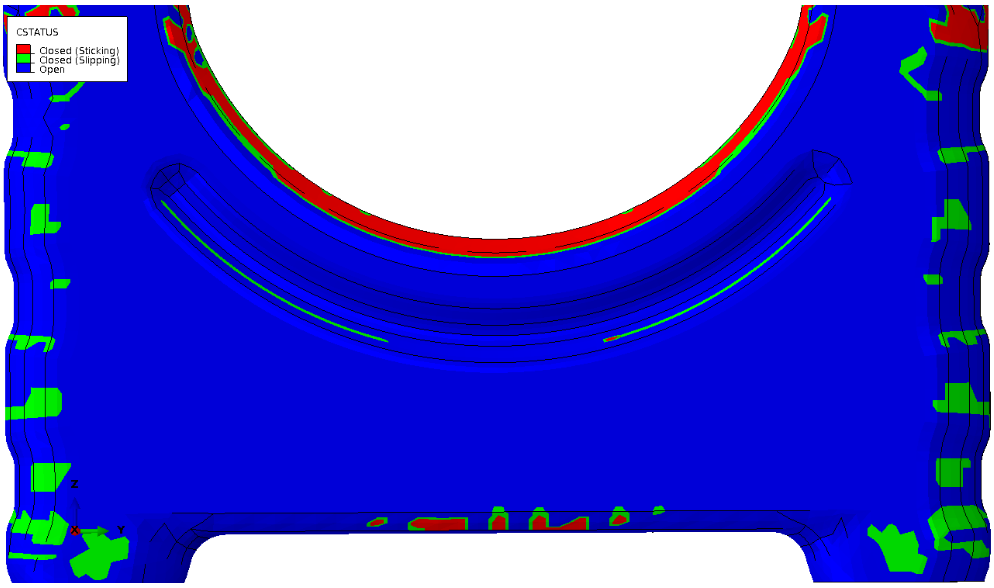

(b)

Figure 4.5: The top figure, (a), shows the contact status between the main bearing supports, with the *Double Groove* design, while the bottom figure, (b), shows a front view of the main bearing support #3. The red areas indicate that the surfaces of the main bearing supports are sticking to the bedplate. The green areas indicate that the surfaces of the main bearing supports are slipping on the bedplate. The blue areas indicate that the surfaces of the main bearing supports and the bedplate are seperated.

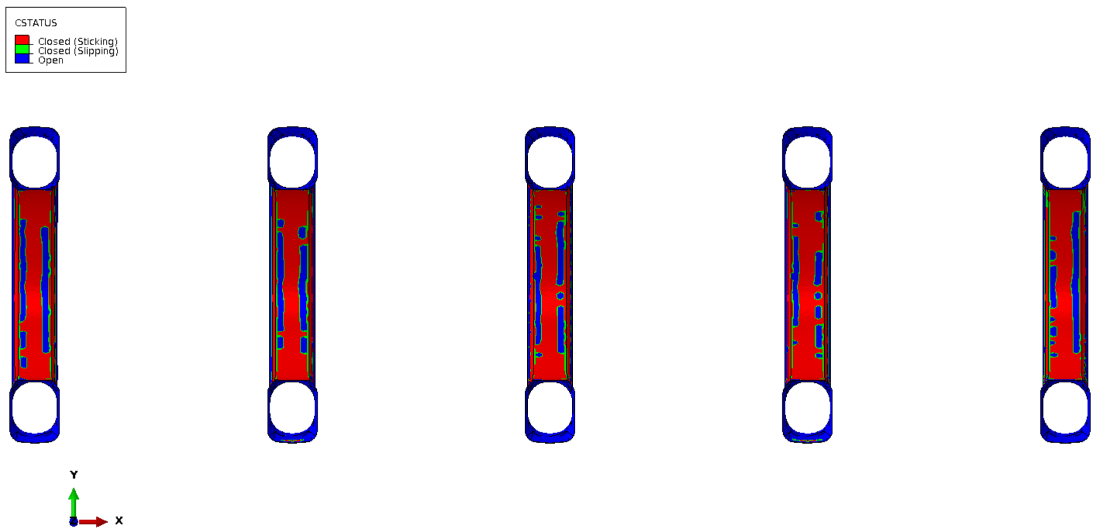

(a)

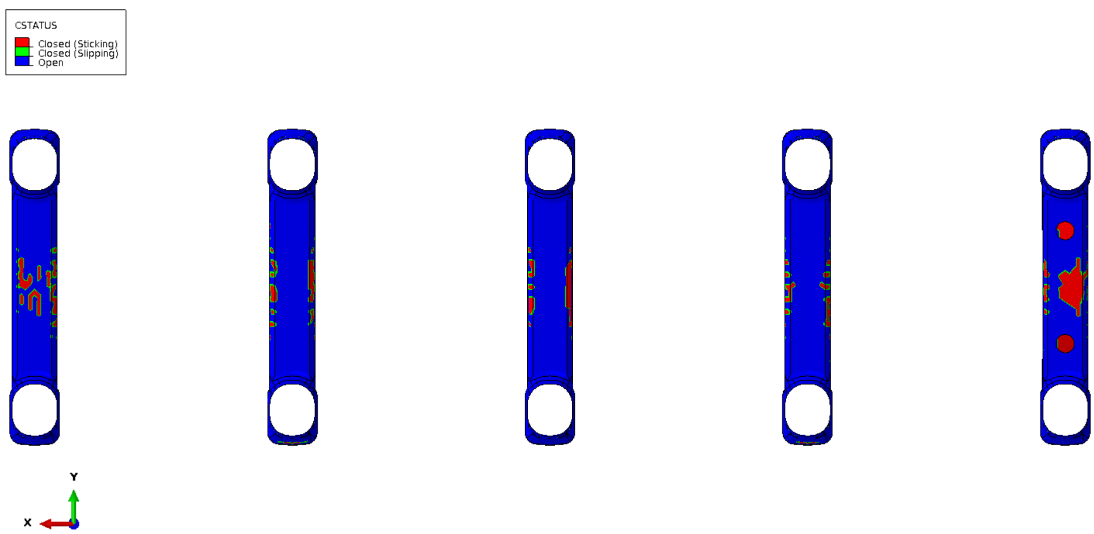

(b)

Figure 4.6: The top figure, (a), shows a top view of the contact status between the main bearing supports, with the *Double Groove* design, while the bottom figure, (b), shows a bottom view of the contact status between the bedplate and the main bearing supports. The red areas indicate that the surfaces of the main bearing supports are sticking to the bedplate. The green areas indicate that the surfaces of the main bearing supports are slipping on the bedplate. The blue areas indicate that the surfaces of the main bearing supports and the bedplate are seperated.

4.2.4 Combination of Grooves

Combination of Grooves shows similar areas of the main bearing supports, where there is any bonding with the bedplate, as with *Double Groove* and *Upper Groove*. This is confirmed when observing Figure 4.7 and Figure 4.8 .

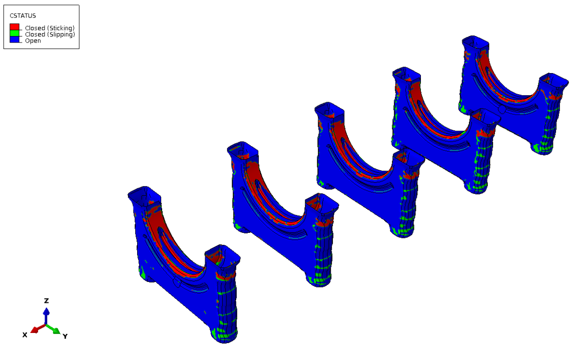

(a)

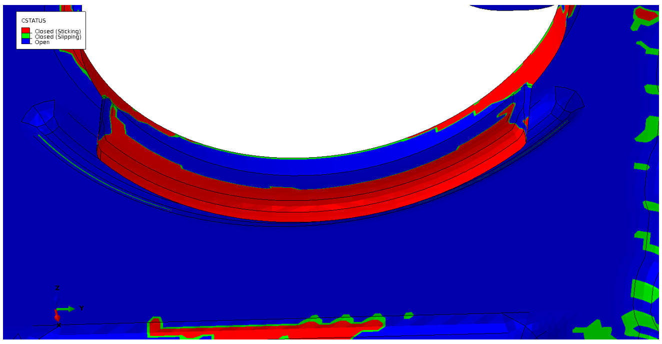

(b)

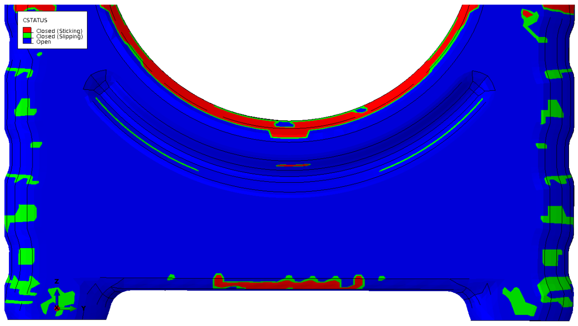

(c)

Figure 4.7: The top figure, (a), shows the contact status between the main bearing supports, with the *Double Groove* design, while the middle figure, (b), shows a cutsection view of the main bearing support #3 and shown in the bottom figure, (c), is a front view of the main bearing support #3 . The red areas indicate that the surfaces of the main bearing supports are sticking to the bedplate. The green areas indicate that the surfaces of the main bearing supports are slipping on the bedplate. The blue areas indicate that the surfaces of the main bearing supports and the bedplate are seperated.

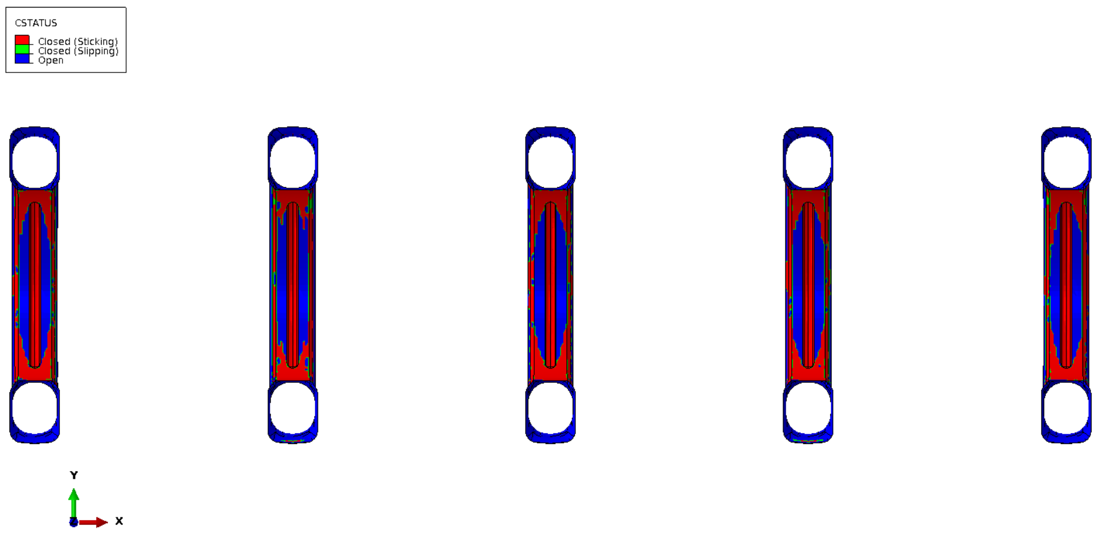

(a)

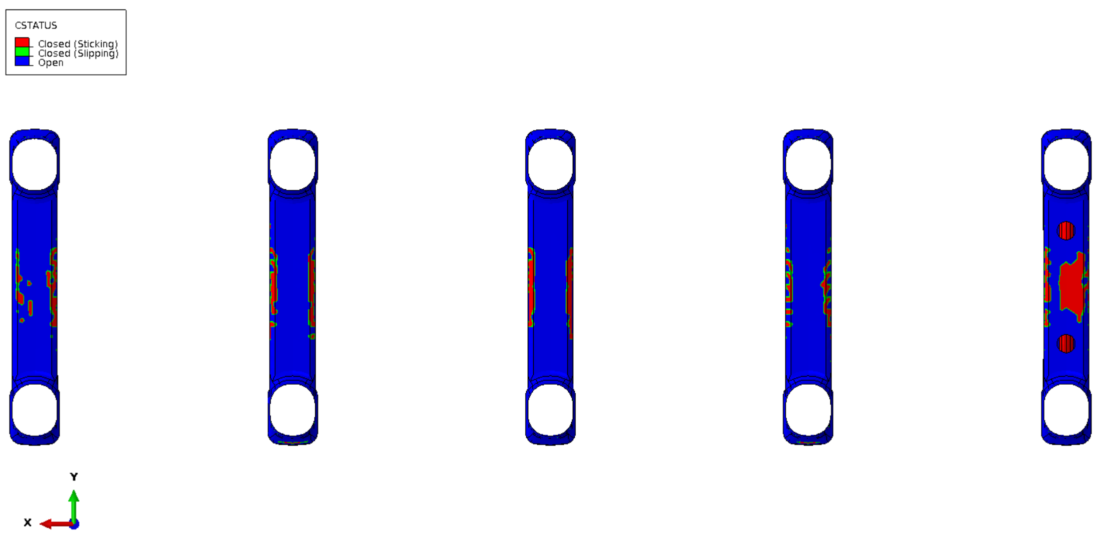

(b)

Figure 4.8: The top figure, (a), shows a top view of the contact status between the main bearing supports, with the *Combination of Grooves* design, while the bottom figure, (b), shows a bottom view of the contact status between the bedplate and the main bearing supports. The red areas indicate that the surfaces of the main bearing supports are sticking to the bedplate. The green areas indicate that the surfaces of the main bearing supports are slipping on the bedplate. The blue areas indicate that the surfaces of the main bearing supports and the bedplate are seperated.

4.3 Mean total friction losses

The total friction loss is the sum of the friction loss caused by the asperity contact between the crankshaft and the bearing shells, and by the pressure and shear flow of the lubricant. The total friction loss was computed at every other degree of the crank angle. For the performance of the main bearings the mean total friction loss during one engine cycle was computed for each main bearing and for the different designs of the main bearing supports, including the sprayed main bearing supports. The results were compared to each other for the engine rotational speeds: 1000 rpm, 2000 rpm and 4000 rpm in various bar diagrams and tables. These are presented in this section. Sprayed main bearing supports will henceforth be referred to as *Spray*.

4.3.1 Mean total friction losses at 1000 rpm

In Figure 4.9 it can be observed that with *Spray*, the mean total friction loss are the lowest for all the main bearings, compared to the other design proposals. One exception is for MB5, where *Combination of Grooves* has the same mean total friction loss as *Spray*. Another observable trend is that *Upper Groove* provide the highest mean total friction losses for all the main bearings compared to the other main bearing support designs. The difference is particularly great, when comparing to *Spray*, with over 15% higher mean total friction loss for four out of five main bearings, as can be observed in Table 4.1. *Double Groove* has the second highest mean total friction loss for all the main bearing, except for MB3, where it has the same mean total friction loss as for *Combination of Grooves*. *Combination of Grooves* and *Al-pillar* has the same mean total friction loss for MB1 and MB2 and has nearly the same for MB3 and MB5.

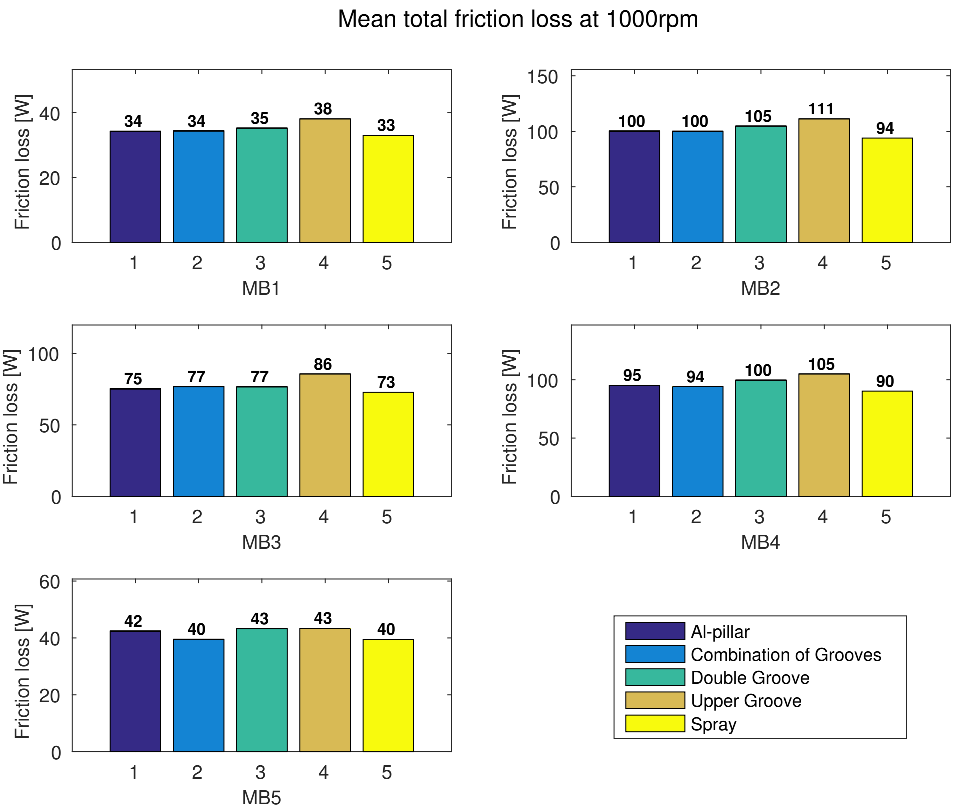

Figure 4.9: Comparison of the mean total friction loss at 1000 rpm for each MB and with the different designs of the main bearing supports

	Spray	Al-pillar	C.o.G	Double Groove	Upper Groove
MB1	Ref	+3.0 %	+3.0 %	+6.1 %	15.2 %
MB2	Ref	+6.4 %	+6.4 %	+11.7 %	+18.1 %
MB3	Ref	+2.7 %	+5.5 %	+5.5 %	17.8 %
MB4	Ref	+5.6 %	+4.4 %	+11.1 %	+16.7 %
MB5	Ref	+5.0 %	+0.0 %	+7.5 %	+7.5 %

Table 4.1: Table showing the relative difference of the mean total friction loss for the design proposals compared to *Spray*, indicated as "Ref", for each main bearing at 1000 rpm.

4.3.2 Mean total friction losses at 2000 rpm

In Figure 4.10, it can be observed that *Spray* provide the lowest mean total friction loss for all the main bearings, except for MB5 where *Combination of Grooves* provide the lowest mean total friction loss. The relative difference in terms of mean total friction loss has also increased, when comparing the design proposals as can be seen in Table 4.2. *Upper Groove* provide the highest mean total friction loss for all the main bearings, except for MB4 and MB5 where *Double Groove* has the same mean total friction loss for MB4 and higher mean total friction loss for MB5.

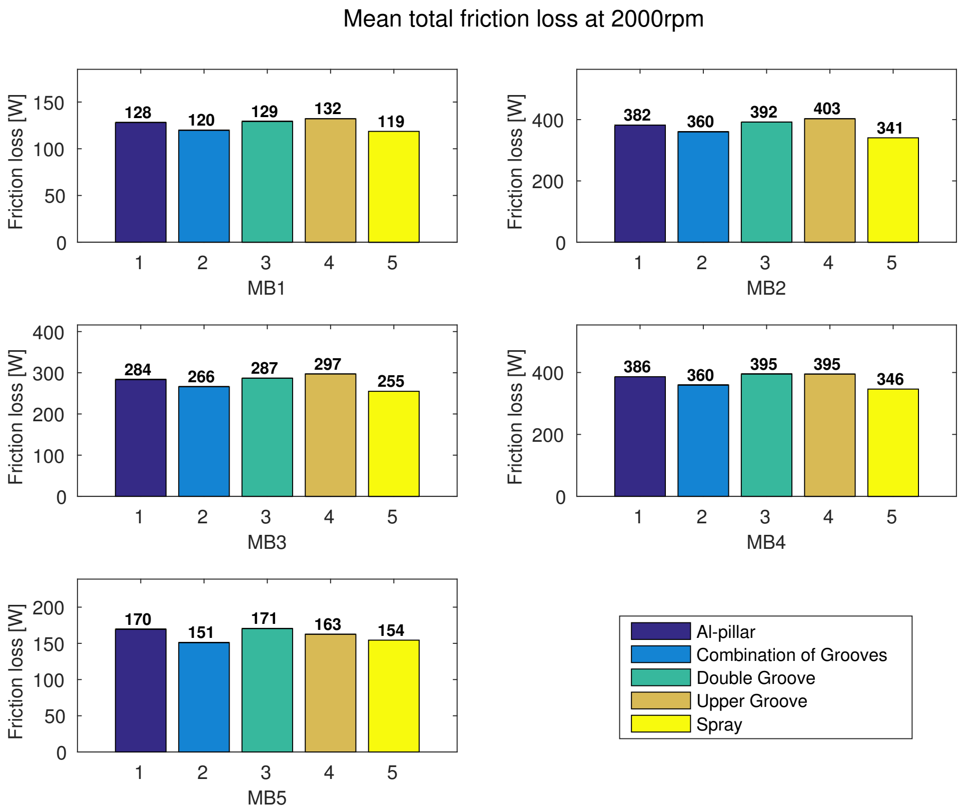

Figure 4.10: Comparison of the mean total friction loss at 2000 rpm for each MB and with the different designs of the main bearing supports

	Spray	Al-pillar	C.o.G	Double Groove	Upper Groove
MB1	Ref	+7.6 %	+0.8 %	+8.4 %	+10.9 %
MB2	Ref	+12.0 %	+5.6 %	+15.0 %	+18.2 %
MB3	Ref	+11.4 %	+4.3 %	+12.5 %	+16.5 %
MB4	Ref	+11.6 %	+4.0 %	+14.2 %	+14.2 %
MB5	Ref	+10.4 %	-1.95 %	+11.04 %	+5.84 %

Table 4.2: Table showing the relative difference of the mean total friction loss for the design proposals compared to *Spray*, indicated as "Ref", for each main bearing at 2000 rpm.

4.3.3 Mean total friction losses at 4000 rpm

In Figure 4.11, it can be observed that *Spray* provide the lowest mean total friction loss for all the main bearings, except for MB1 where *Al-pillar* and *Upper Groove* provide the lowest mean total friction loss. For the other main bearings, the *Combination of Grooves* provide the second lowest mean total friction loss, with a very small relative difference compared to *Spray* for MB1, MB2 and MB5, as observed in Table 4.3

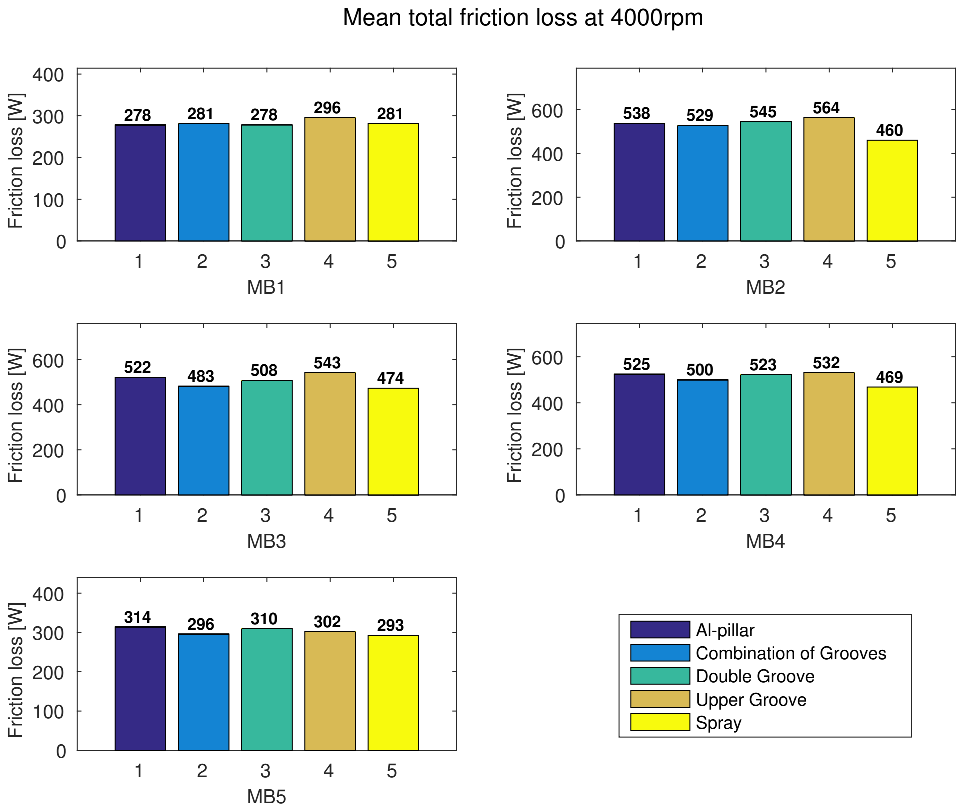

Figure 4.11: Comparison of the mean total friction loss at 4000 rpm for each MB and with the different designs of the main bearing supports.

	Spray	Al-pillar	C.o.G	Double Groove	Upper Groove
MB1	Ref	-1.07 %	+0.0 %	-1.07 %	+5.34 %
MB2	Ref	+17.0 %	+15.0 %	+18.5 %	+22.6 %
MB3	Ref	+10.1 %	+1.9 %	+7.2 %	+14.6 %
MB4	Ref	+11.9 %	+6.6 %	+11.5 %	+13.4 %
MB5	Ref	+7.2 %	+1.0 %	+5.8 %	+3.1 %

Table 4.3: Table showing the relative difference of the mean total friction loss for the design proposals compared to *Spray*, indicated as "Ref", for each main bearing at 4000 rpm.

4.4 Maximum total pressure

The maximum total pressure is made up of the pressure from the lubricant and the asperity contact pressure. Figures showing the maximum total pressure for each main bearing and for each design of the main bearing supports at the engine rotational speeds: 1000 rpm, 2000 rpm and 4000 rpm can be observed in Appendix B.

4.5 Maximum asperity contact pressure

In this section the maximum asperity contact pressure on the main bearings for the engine rotational speeds: 1000 rpm, 2000 rpm and 4000 rpm are shown in various figures. The maximum asperity contact pressure is computed for every other crank angle over two engine cycles for each main bearing. The results are compared for each design proposal with *Spray* as follows:

- *Combination of Grooves* and *Al-pillar* compared with *Spray*
- *Double Groove* and *Upper Groove* compared with *Spray*.

4.5.1 The maximum asperity contact pressure at 1000 rpm

In Figure 4.12, it can be observed that for all the main bearings *Spray* has larger areas of high pressure, 96-120 MPa, compared to *Combination of Grooves* and *Al-pillar*. We can also observe in Table 4.4 that for all the main bearings, except for MB2, *Spray* has the highest asperity contact pressure in middle area of the lower bearing shell. *Combination of Grooves* has the highest asperity contact pressure at the edges of MB1, MB4 and MB5 as observed in Table 4.5.

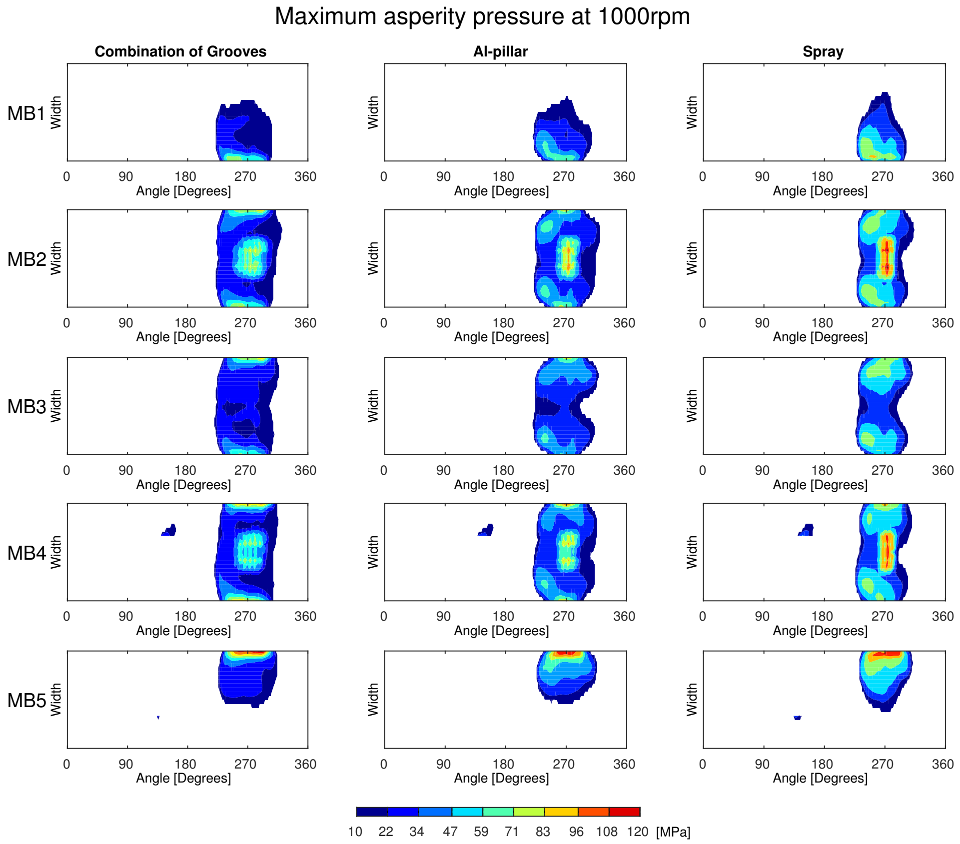

Figure 4.12: The maximum asperity contact pressure at 1000 rpm shown for all the main bearings unwrapped. Each column represents the designs of main bearing supports. From left to right is *Combination of Grooves*, *Al-pillar* and *Spray*.

	C.o.G	Al-pillar	Spray
MB1	63.21 MPa	80.36 MPa	86.27 MPa
MB2	98.56 MPa	111.44 MPa	110.45 MPa
MB3	74.94 MPa	88.34 MPa	102.59 MPa
MB4	75.64 MPa	85.59 MPa	92.15 MPa
MB5	72.88 MPa	85.62 MPa	95.06 MPa

Table 4.4: Table showing the maximum asperity contact pressure in the middle of the lower main bearing shells for the design proposals: *Combination of Grooves*, shortened to the initials C.o.G, *Al-pillar* and *Spray* at 1000 rpm.

	C.o.G	Al-pillar	Spray
MB1	88.38 MPa	81.51 MPa	87.34 MPa
MB2	87.22 MPa	86.62 MPa	96.48 MPa
MB3	92.74 MPa	85.33 MPa	96.23 MPa
MB4	94.72 MPa	89.60 MPa	90.54 MPa
MB5	122.61 MPa	113.20 MPa	110.07 MPa

Table 4.5: Table showing the maximum asperity contact pressure at the edges of the lower main bearing shells for the design proposals: *Combination of Grooves*, shortened to the initials C.o.G, *Al-pillar* and *Spray* at 1000 rpm.

In Figure 4.13 it can be observed that *Double Groove* does not show areas of high asperity contact pressure, 96-120 MPa, in the middle of the lower main bearing shell of MB2 and MB4, unlike the other designs of the main bearing supports. *Double Groove* also show larger areas of high asperity contact pressure, 96-120 MPa, for MB1 and MB5. For *Upper Groove* the areas of high asperity contact pressure, 96-120 MPa, are very small compared to *Double Groove* and *Spray*. In Table 4.6 and 4.7 it can be observed that *Spray* has the largest asperity contact pressure for all the main bearings.

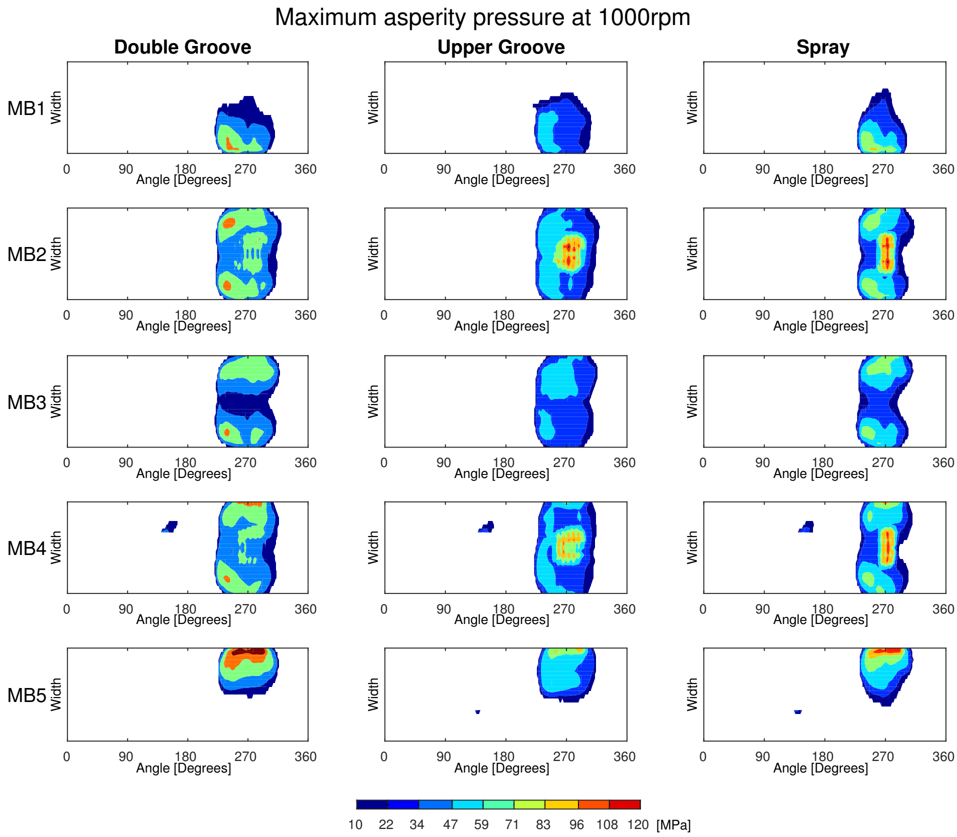

Figure 4.13: The maximum asperity contact pressure at 1000 rpm shown for all the main bearings unwrapped. Each column represents the designs of main bearing supports. From left to right is *Double Groove*, *Upper Groove* and *Spray*

	Double Groove	Upper Groove	Spray
MB1	80.57 MPa	77.32 MPa	86.27 MPa
MB2	85.69 MPa	109.05 MPa	110.45 MPa
MB3	87.81 MPa	85.03 MPa	102.59 MPa
MB4	88.97 MPa	85.84 MPa	92.15 MPa
MB5	85.88 MPa	82.90 MPa	95.06 MPa

Table 4.6: Table showing the maximum asperity contact pressure in the middle of the lower main bearing shells for the design proposals: *Double Groove*, *Upper Groove* and *Spray* at 1000 rpm.

	Double Groove	Upper Groove	Spray
MB1	80.97 MPa	73.60 MPa	87.34 MPa
MB2	84.89 MPa	75.13 MPa	96.48 MPa
MB3	85.62 MPa	75.42 MPa	96.23 MPa
MB4	87.31 MPa	78.39 MPa	90.54 MPa
MB5	95.60 MPa	89.49 MPa	110.07 MPa

Table 4.7: Table showing the maximum asperity contact pressure at the edges of the lower bearing shells for the design proposals: *Double Groove*, *Upper Groove* and *Spray* at 1000 rpm.

4.5.2 Maximum asperity contact pressure at 2000 rpm

In Figure 4.14, it can be observed that *Al-pillar* has significantly larger areas of high asperity contact pressure, 173-220 MPa, in the middle of the lower bearing shell of MB2 and MB4, compared to *Spray* and *Combination of Grooves*. *Al-pillar* also has a larger area of high asperity contact pressure, 173-220 MPa, at the edges of MB5. In Table 4.8, we can observe that *Spray* has the highest maximum asperity contact pressure in the middle of the lower bearing shell for all the main bearings compared to *Combination of Grooves* and *Al-pillar*. *Combination of Groove* shows the highest maximum asperity contact pressure at the edges compared to *Spray* and *Al-pillar*.

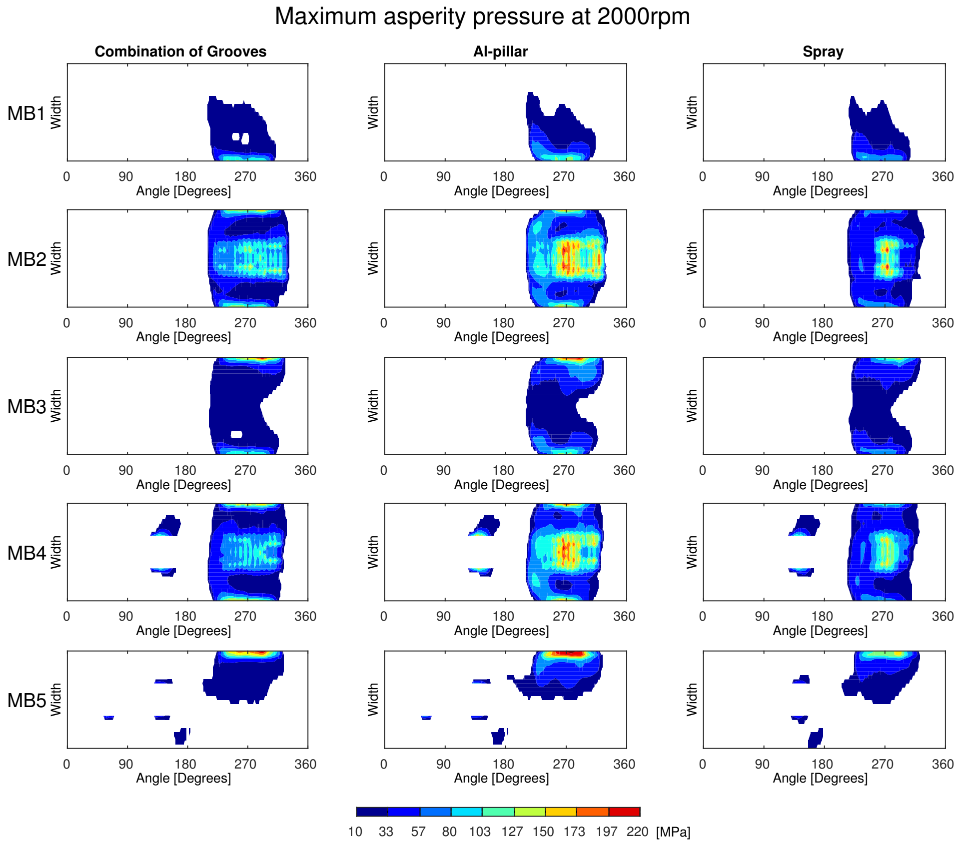

Figure 4.14: The maximum asperity contact pressure at 2000 rpm shown for all the main bearings unwrapped. Each column represents the designs of the main bearing supports. From left to right is *Combination of Grooves*, *Al-pillar* and *Spray* at 2000 rpm

	C.o.G	Al-pillar	Spray
MB1	84.25 MPa	105.47 MPa	111.96 MPa
MB2	133.63 MPa	152.18 MPa	212.85 MPa
MB3	97.14 MPa	110.93 MPa	128.22 MPa
MB4	132.34 MPa	135.49 MPa	161.86 MPa
MB5	95.63 MPa	109.97 MPa	120.80 MPa

Table 4.8: Table showing the maximum asperity contact pressure in the middle of the lower main bearing shells for the design proposals: *Combination of Grooves*, shortened to the initials C.o.G, *Al-pillar* and *Spray* at 2000 rpm.

	C.o.G	**Al-pillar**	**Spray**
MB1	133.26 MPa	116.17 MPa	123.13 MPa
MB2	154.13 MPa	114.17 MPa	117.06 MPa
MB3	208.20 MPa	156.31 MPa	169.63 MPa
MB4	156.00 MPa	134.56 MPa	122.73 MPa
MB5	229.34 MPa	196.85 MPa	211.85 MPa

Table 4.9: Table showing the maximum asperity contact pressure at the edges of the lower main bearing shell for the design proposals: *Combination of Grooves*, shortened to the initials C.o.G, *Al-pillar* and *Spray* at 2000 rpm.

In Figure 4.15, we can observe that *Upper Groove* has a significantly larger area of high asperity contact pressure, 173-220 MPa, in the middle of the lower bearing shell of MB2 and MB4 compared to *Double Groove* and *Spray.* If we look at Table 4.10, we can observe that *Spray* has the highest maximum asperity contact pressure in the middle of the lower bearing shell compared to *Double Groove* and *Upper Groove* for all the main bearings, except for MB4 where *Upper Groove* has the highest maximum asperity contact pressure. *Spray* also has the highest maximum asperity contact pressure at the edges of all the main bearings, as can be observed in Table 4.11. *Double Groove* shows a larger area of high asperity contact pressure, 150-173 MPa, at the edge of the lower bearing shell of MB5 compared to *Upper Groove* and *Spray.*

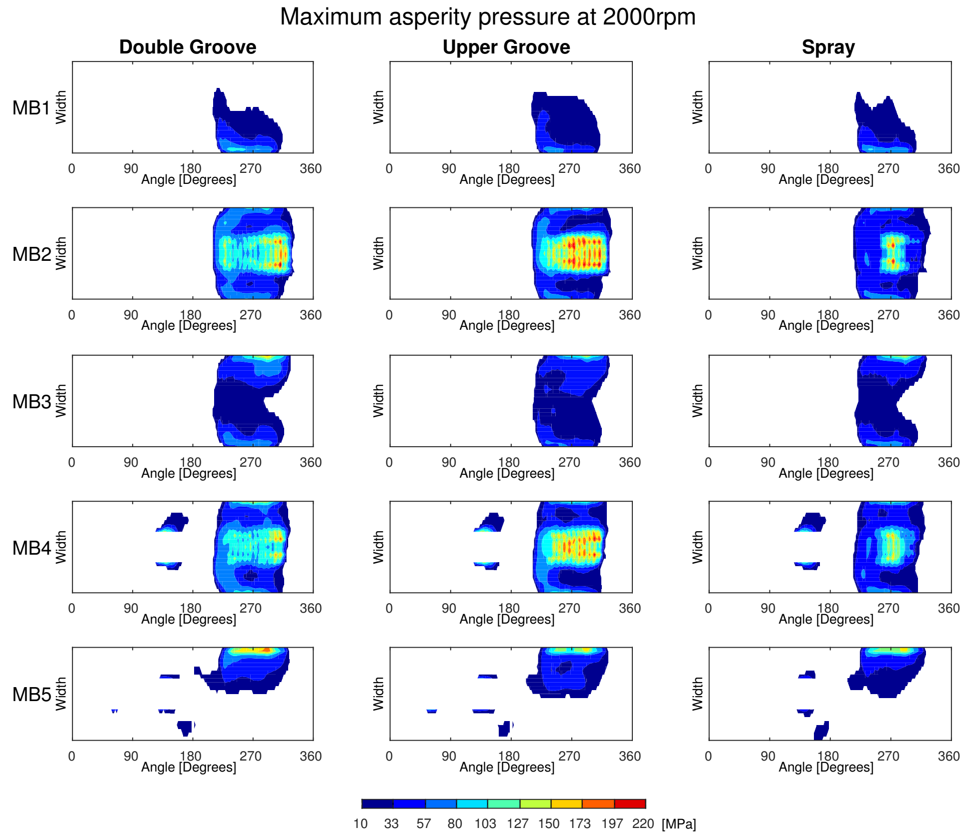

Figure 4.15: The maximum asperity contact pressure at 2000 rpm shown for all the main bearings unwrapped. Each column represents the designs of main bearing supports. From left to right is *Double Groove*, *Upper Groove* and *Spray*

	Double Groove	Upper Groove	Spray
MB1	103.86 MPa	100.79 MPa	111.96 MPa
MB2	156.67 MPa	184.19 MPa	212.85 MPa
MB3	112.03 MPa	111.17 MPa	128.22 MPa
MB4	132.49 MPa	162.56 MPa	161.86 MPa
MB5	112.00 MPa	107.98 MPa	120.80 MPa

Table 4.10: Table showing the maximum asperity contact pressure in the middle of the lower main bearing shells for the design proposals: *Double Groove*, *Upper Groove* and *Spray* at 2000 rpm.

	Double Groove	**Upper Groove**	**Spray**
MB1	102.97 MPa	97.33 MPa	123.13 MPa
MB2	109.48 MPa	102.12 MPa	117.06 MPa
MB3	147.48 MPa	126.95 MPa	169.63 MPa
MB4	119.57 MPa	109.94 MPa	122.73 MPa
MB5	181.49 MPa	168.84 MPa	211.85 MPa

Table 4.11: Table showing the maximum asperity contact pressure at the edges of the lower main bearing shells for the design proposals: *Double Groove*, *Upper Groove* and *Spray* at 2000 rpm.

4.5.3 Maximum asperity contact pressure at 4000 rpm

In Figure 4.16, we can observe that *Spray* has larger areas of high asperity contact pressure, 150-190 MPa, for the lower bearing shell of MB2 and MB4 compared to *Combination of Grooves* and *Al-pillar*. If we look at Table 4.12 we can also observe that *Spray* has the highest maximum asperity contact pressure in the middle of the lower bearing shell of MB2, MB3 and MB4 while *Combination of Grooves* has the highest maximum asperity contact pressure in the middle of the lower bearing shell of MB1 and MB5. We can observe in Figure 4.16 that *Combination of Grooves* shows larger areas of high asperity contact pressure, 130-170 MPa, at the edges of MB1 and MB5 compared to *Al-pillar* and *Spray*. In Table 4.13 we can also observe that *Combination of Grooves* has the highest maximum asperity contact pressure at the edges of the lower bearing shell of all the main bearings, except for MB1 where *Spray* has the highest maximum asperity contact pressure.

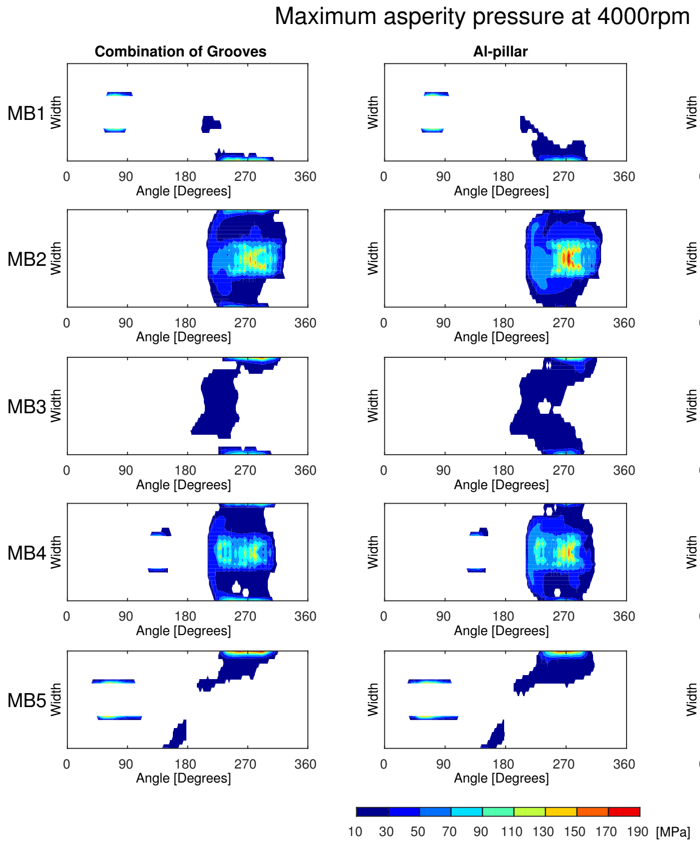

Figure 4.16: The maximum asperity contact pressure at 4000 rpm shown for all the main bearings unwrapped. Each column represents the designs of main bearing supports. From left to right is *Combination of Grooves*, *Al-pillar* and *Spray*

	C.o.G	Al-pillar	Spray
MB1	129.09 MPa	119.96 MPa	115.54 MPa
MB2	127.31 MPa	140.85 MPa	184.80 MPa
MB3	91.25 MPa	102.06 MPa	119.67 MPa
MB4	110.27 MPa	113.96 MPa	146.24 MPa
MB5	148.42 MPa	135.54 MPa	127.18 MPa

Table 4.12: Table showing the maximum asperity contact pressure in the middle of the lower main bearing shells for the design proposals: *Combination of Grooves*, shortened to the initials C.o.G, *Al-pillar* and *Spray* at 4000 rpm.

	C.o.G	Al-pillar	Spray
MB1	120.42 MPa	110.31 MPa	121.04 MPa
MB2	114.10 MPa	103.40 MPa	103.52 MPa
MB3	144.05 MPa	117.78 MPa	126.59 MPa
MB4	113.23 MPa	101.30 MPa	107.02 MPa
MB5	162.18 MPa	157.02 MPa	151.11 MPa

Table 4.13: Table showing the maximum asperity contact pressure at the edges of the lower main bearing shells for the design proposals: *Combination of Grooves*, shortened to the initials C.o.G, *Al-pillar* and *Spray* at 4000 rpm.

In Figure 4.17 we can observe that *Spray* shows larger regions of high asperity contact pressure, 150-190 MPa, in the middle of the lower bearing shell of MB2 and MB4 compared to *Double Groove* and *Upper Groove*. In Table 4.14 we can observe that *Spray* has the highest maximum asperity contact pressure in the middle of the lower bearing shell for all the main bearings compared to *Double Groove* and *Upper Groove*. *Spray* has the highest maximum asperity contact pressure at the edges of the lower bearing shell of MB2, MB3 and MB4 while *Upper Groove* shows the highest maximum asperity contact pressure for MB1 and MB5 as can be observed in Table 4.15.

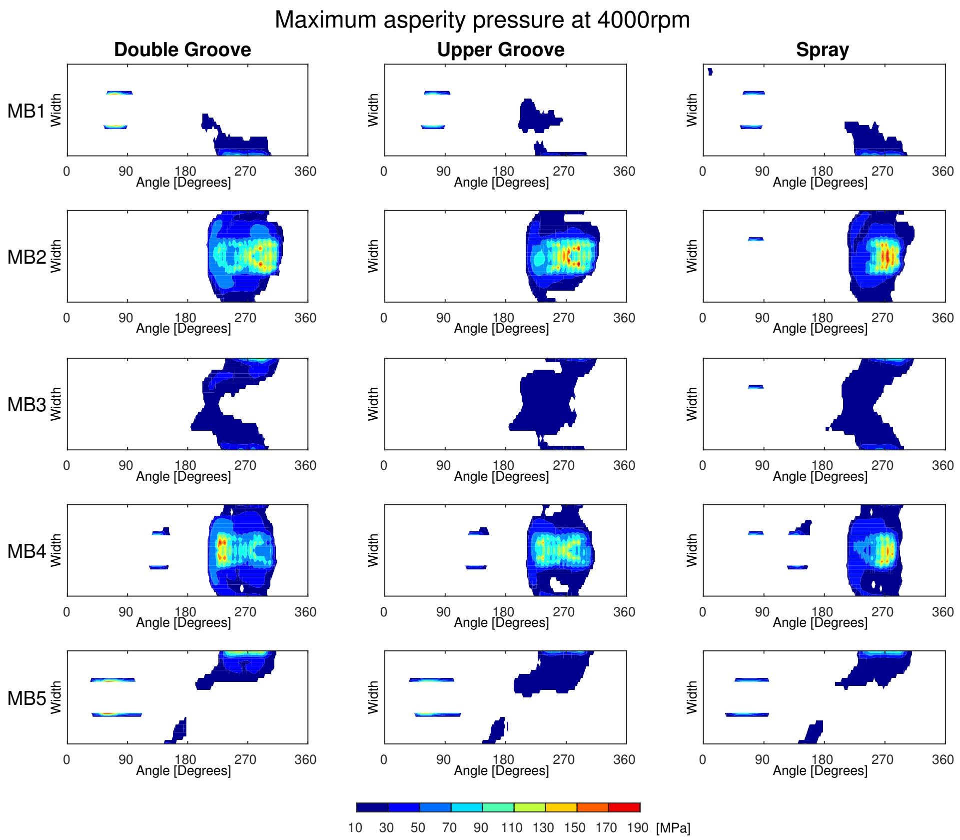

Figure 4.17: The maximum asperity contact pressure at 4000 rpm shown for all the main bearings unwrapped. Each column represents the designs of main bearing supports. From left to right is *Double Groove*, *Upper Groove* and *Spray*

	Double Groove	Upper Groove	Spray
MB1	104.08 MPa	103.01 MPa	121.04 MPa
MB2	100.74 MPa	98.92 MPa	103.52 MPa
MB3	107.57 MPa	103.06 MPa	126.59 MPa
MB4	104.43 MPa	100.95 MPa	107.02 MPa
MB5	134.51 MPa	120.39 MPa	151.11 MPa

Table 4.14: Table showing the maximum asperity contact pressure in the middle of the lower main bearing shells for the design proposals: *Double Groove*, *Upper Groove* and *Spray* at 4000 rpm.

	Double Groove	Upper Groove	Spray
MB1	120.02 MPa	132.89 MPa	115.54 MPa
MB2	118.63 MPa	177.40 MPa	184.80 MPa
MB3	100.57 MPa	104.01 MPa	119.67 MPa
MB4	111.71 MPa	135.27 MPa	146.24 MPa
MB5	135.91 MPa	148.56 MPa	127.18 MPa

Table 4.15: Table showing the maximum asperity contact pressure at the edges of the lower main bearing shells for the design proposals: *Double Groove*, *Upper Groove* and *Spray* at 4000 rpm.

5
Discussion

5.1 Methodology

The mesh size used in *ABAQUS* was smaller than the one used in *Excite PU*. It was therefore not possible to properly paste the elements of bedplate, which were in contact with the main bearing supports, according to the contact status from the *ABAQUS*-analyses. It would have been more favourable to use the same mesh in *ABAQUS* and *Excite PU*, but it would also have meant more work since it would have been necessary to redo most of the pre processing for other parts of the model of the engine used in *Excite PU*.

5.2 Results

The grooves on the front and back face of *Combination of Grooves* and *Doube Groove* provided a small contact area with the bedplate. This could be due to the curvature of the grooves being too rounded. For *Upper Groove*, the whole top surfaces of the main bearing supports were sticking to the bedplate, unlike *Coombination of Grooves* and *Upper Groove*. This questions the necessity of making a groove on the top surfaces of the main bearing support, as was done for *Upper Groove* and *Combination of Grooves*.

As mentioned in the introduction, the cost of spraying the main bearing supports, with the aluminium alloy AlSI12, is high. But this shouldn't exclude a design proposal where less of the coating material is used. For instance, the front and back face of the main bearing supports could be sprayed with the aluminium alloy and still achieve a strong bonding with the bedplate and thereby provide a more smooth distribution of asperity contact pressure on the main bearings and avoid high asperity contact pressure at the edges of the lower bearing shell of each main bearing. The bonding between the bedlate and the main bearing supports also appear to have an effect on the friction losses on the main bearings. *Spray* clearly showed the lowest mean total friction loss for almost every main bearing and engine rotational speed. The design proposal that came closest to the levels of friction loss that *Spray* had, was *Combination of Grooves*.

6

Conclusions & Future work

The mean total friction losses for the different design proposals could not be matched with the sprayed main bearing supports. There were few exceptions to this for certain main bearings at certain engine rotational speeds. Table 6.1 shows the average of all the main bearings' mean total friction for the different designs of the main bearing support at different engine rotational speeds and Table 6.2 shows the relative difference between the design proposals and *Spray*.

RPM	**Spray**	**Al-pillar**	**C.o.G**	**Double Groove**	**Upper Groove**
1000	330 W	346 W	345 W	360 W	383 W
2000	1215 W	1350 W	1258 W	1374 W	1390 W
4000	1977 W	2177 W	2089 W	2164 W	2237 W

Table 6.1: Table showing the average of all the main bearings' mean total friction losses at different engine speeds, for the different designs of the main bearing supports. Note: C.o.G stands for *Combination of Grooves*.

RPM	**Spray**	**Al-pillar**	**C.o.G**	**Double Groove**	**Upper Groove**
1000	Ref	+4.8 %	+4.5 %	+9.1 %	+16.1 %
2000	Ref	+11.1 %	+3.5 %	+13.1 %	+14.4 %
4000	Ref	+10.1 %	+5.7 %	+9.5 %	+13.2 %

Table 6.2: Table showing the relative difference of the average of all the main bearings' mean total friction at different engine rotational speeds speeds for the design proposals compared to *Spray*. Note, C.o.G stands for *Combination of Grooves*.

In Table 6.3, we can see that *Combination of Grooves* has the highest average of the main bearings' maximum asperity contact pressure at the edges of any lower bearing shell for the engine rotational speeds. While *Spray* has the highest mean asperity contact pressure at the center of any lower bearing shell at the different engine speeds shown in Table 6.4.

RPM	Spray	Al-pillar	C.o.G	Double Groove	Upper Groove
1000	95.92 MPa	91.02 MPa	97.13 MPa	86.80 MPa	79.15 MPa
2000	148.88 MPa	143.61 MPa	176.19 MPa	132.20 MPa	121.04 MPa
4000	121.86 MPa	117.96 MPa	130.80 MPa	110.27 MPa	105.27 MPa

Table 6.3: Table showing the mean values of all the main bearings' maximum asperity contact pressure at the edges of the lower bearing shell bearings at different engine rotational speeds and for different designs of the main bearing supports. Note, C.o.G stands for *Combination of Grooves*.

RPM	Spray	Al-pillar	C.o.G	Double Groove	Upper Groove
1000	97.30 MPa	90.27 MPa	77.05 MPa	85.78MPa	88.03 MPa
2000	147.14 MPa	122.81 MPa	108.60 MPa	123.41 MPa	133.34 MPa
4000	138.69 MPa	122.47 MPa	121.27 MPa	117.37 MPa	139.63 MPa

Table 6.4: Table showing the mean values of all the main bearings' maximum asperity contact pressure in the middle of the lower bearing shell, for all the main bearings at different engine rotational speeds and for different designs of the main bearing supports. Note, C.o.G stands for *Combination of Grooves* and "Ref" stands for the reference value.

6.1 Future work

Besides friction losses in the main bearings and the risk of wearing down the main bearings, it is also important to investigate the risk of having a fatigue failure in the bedplate when running the engine at different load cases. The fatigue can occur as a result of high amplitude stress, due to the loads from the crankshaft and due to the temperature load of the running the engine. As stated in the introduction the reason for spraying the main bearing supports with an aluminium alloy coating was to provide better bonding between the bedplate and the main bearing supports. In order to investigate if there could be a risk of having fatigue problems in the bedplate, with the different design proposals, the equivalent plastic strain was checked at the operating temperature of the engine, 130 °C. The two design proposals *Al-pillar* and *Combination of Grooves* was selected and compared to *Spray*. Figure 6.1 reveals that *Combination of Grooves* has large plastic strains around the corners especially the ones at the bottom. This is similar to Figure 6.2 where *Al-pillar* also has large equivalent plastic strains around the corners, although smaller. Further analysis in this area is therefore necessary, if VCC should proceed with one of the design proposals. Another important issue regarding the design proposals would be the feasibility and the cost of manufacturing a new design of the main bearing support. It would also be a matter of discussing with VCC's current supplier and manufacturer of the main bearing supports and possibly the company spraying the main bearing supports, if VCC would adopt a solution involving spraying the main bearing supports wit the aluminium alloy.

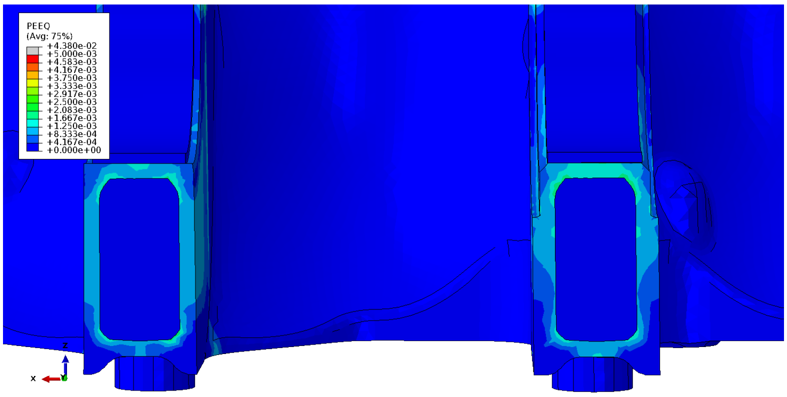

(a)

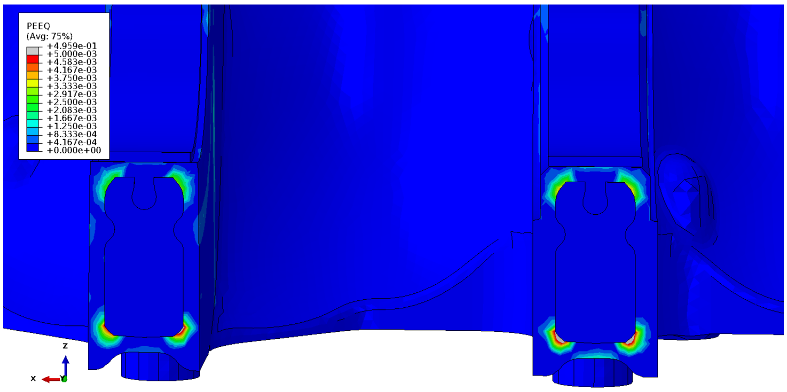

(b)

Figure 6.1: The top figure, (a), shows a cut section view of the bedplate and the main bearing supports with the equivalent plastic strain at 130 °C plotted for *Spray* and in the bottom figure, (b), for *Combination of Grooves*.

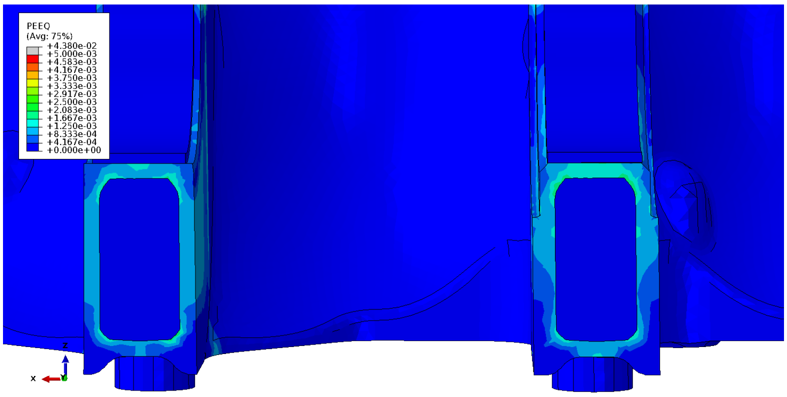

(a)

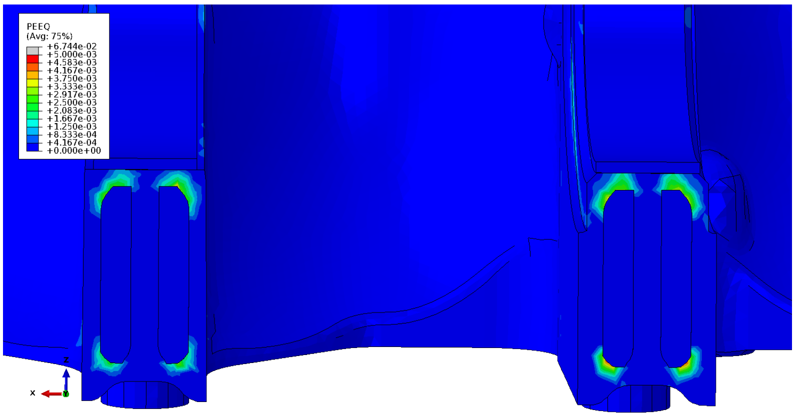

(b)

Figure 6.2: The top figure, (a), shows a cut section view of the bedplate and the main bearing supports with the equivalent plastic strain at 130 °C plotted for *Spray* and in the bottom figure, (b), for *Al-pillar*.

Bibliography

[1] D. Crabb, M. Fleiss, J.-E. Larsson, and J. Somhorst, *New Modular Engine Platform from Volvo*, MTZ worldwide, pp. 4–11, Sep. 2013.

[2] S. Larzenius, Sep. 2016.

[3] S.Larzenius, *Main bearing performance using sprayed vs non-sprayed iron inserts on an I4 diesel engine* presented at AVL-conference in Graz, unpublished, 2015.

[4] Volvo Car Corporation, *Competence Business Development, New Car Training 13W46, Theoretical Session*, Nov. 2013.

[5] Volvo Car Corporation, *VEA Bearing calc data.*

[6] H. Allmaier, C. Priestner, F. M. Reich, H. H. Priebsch, C. Forstner, and F. Novotny-Farkas, *Predicting friction reliably and accurately in journal bearings – The importance of extensive oil-models*, Tribology International, vol. 48, pp. 93–101, Apr. 2012.

[7] K. Mollenhauer, *Handbook of Diesel Engines*, M. Klaus and H. Tschoeke, Eds., 1st ed. Springer, 2010.

[8] G. Offner, *Friction Power Loss Simulation of Internal Combustion Engines Considering Mixed Lubricated Radial Slider, Axial Slider and Piston to Liner Contacts*, Tribology Transactions, vol. 56, no. 3, pp. 503–515, Jan. 2013.

[9] Spurk J. H., Aksel N. *Ströhmungslehre - Einführung in die Theorie der Strömungen, 7.Auflage*, Springer Verlag, 2007.

[10] Krasser J.*Thermoelastohydrodynamische Analyse dynamisch belasteter Radialgleitlager*,Dissertation, 1996.

[11] Offner G.*Mathematische Modellierung des Kolben - Zylinder - Kontakts in Verbrennungskraftma-schinen und numerische Simulation des durch mechanischen Kolbenschlag angeregten Koerperschalls (Mathematical Model of the Piston to Liner Contact in Combustion Engines and Numerical Simulation of the Structure Borne Noise Excited byMechanical Piston Impact)*, PhD Theses, 2000.

[12] AVL List Gmbh, *Theory AVL EXCITE POWER UNIT VERSION 2013.2*, Oct. 30, 2013.

[13] C. Priestner, H. Allmaier, H. H. Priebsch, and C. Forstner, *Refined simulation of friction power loss in crank shaft slider bearings considering wear in the mixed lubrication regime*, Tribology International, vol. 46, no. 1, pp. 200–207, Feb. 2012.

[14] K. L. Hoag, *Vehicular Engine Design*, H. List, Ed., 2nd. Springer, 2016.

[15] Volvo Car Corporation, *Technical Regulation ALUMINIUM SPRAYED BEARING REINFORCEMENTS*, Volvo Car Corporation, May 28, 2012.

[16] BETA CAE Systems, *ANSA v15.3.1*, https://www.beta-cae.com/ansa.htm, 2015.
[17] Dassault Systems, *ABAQUS v6.14-3*,https://www.3ds.com/products-services/simulia/, 2016.
[18] Dassault Systems, *ABAQUS-viewer v6.14-3*, https://www.3ds.com/products-services/simulia/, 2016.
[19] MSC Software, *MSC Nastran 2012.2*, http://www.mscsoftware.com/product/msc-nastran, 2012
[20] AVL, *Excite PU v.2013.2*, https://www.avl.com/excite, 2013.
[21] Mathworks, *MATLAB 2015b*, https://se.mathworks.com/products/matlab.html, 2015
[22] S. Larzenius and H. Johansson, *Private communication* Sep. 2016.
[23] P. Wriggers and T. A. Laursen, Eds., *Computational Contact Mechanics*, 1st ed. Springer, 2007.
[24] R. R. Craig Jr and A. J. Kurdila, *Fundementals of Structural Dynamics*, Second ed. Wiley, 2006.

A

Deformed profiles of the main bearings for the different design proposals

A.1 Al-pillar

A.1.1 Main Bearing 1

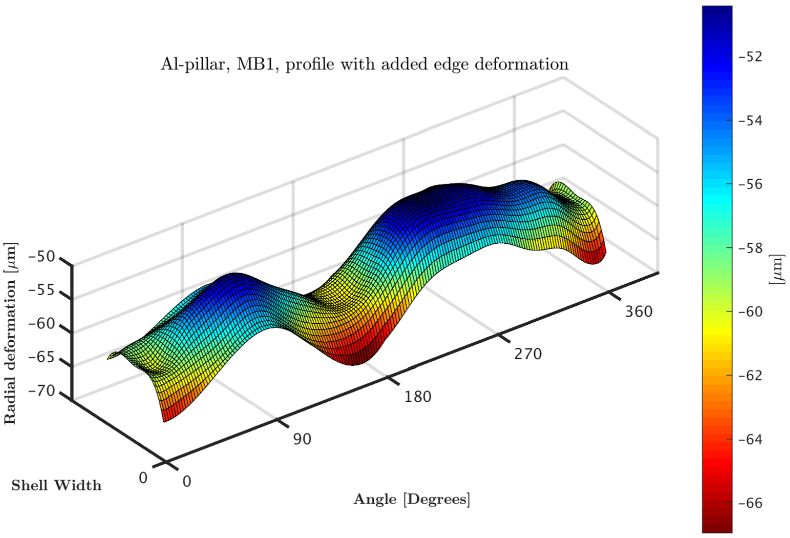

Figure A.1: The radial deformation of the profile of MB1 for *Al-pillar* used in *AVL EXCITE PU*.

A.1.2 Main Bearing 2

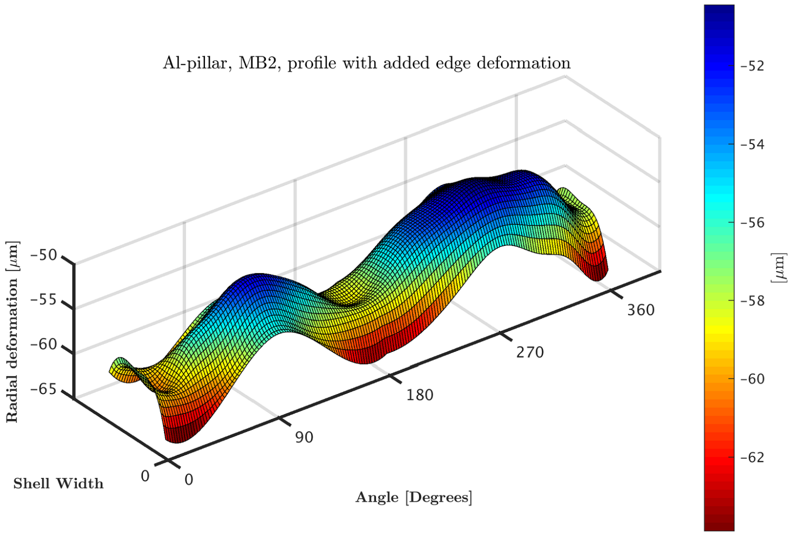

Figure A.2: The radial deformation of the profile of MB2 for *Al-pillar* used in *AVL EXCITE PU*.

A.1.3 Main Bearing 3

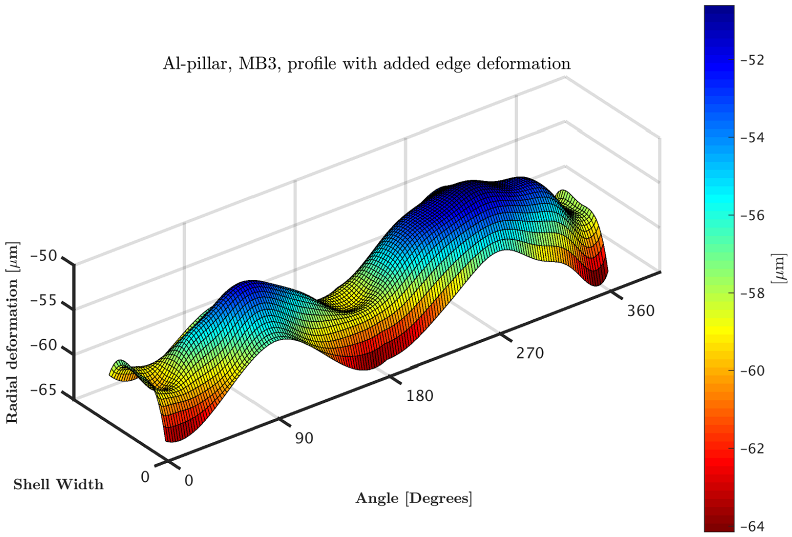

Figure A.3: The radial deformation of the profile of MB3 for *Al-pillar* used in *AVL EXCITE PU*.

A.1.4 Main Bearing 4

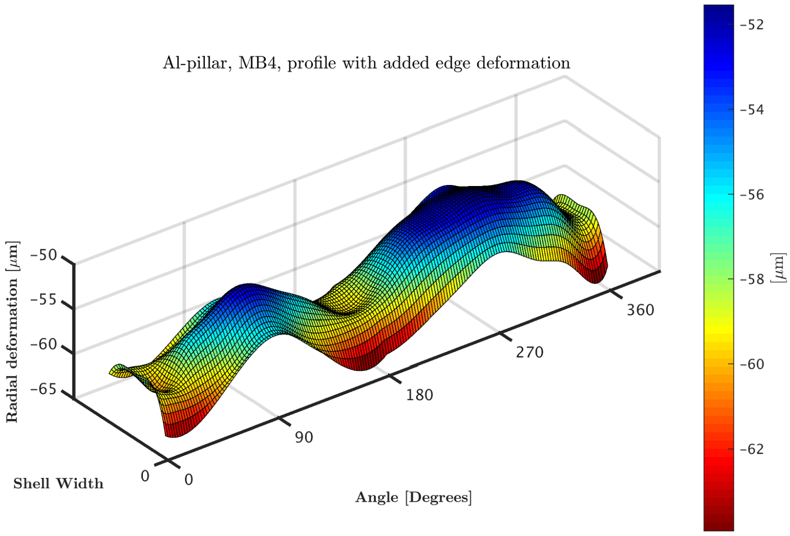

Figure A.4: The radial deformation of the profile of MB4 for *Al-pillar* used in *AVL EXCITE PU*.

A.1.5 Main Bearing 5

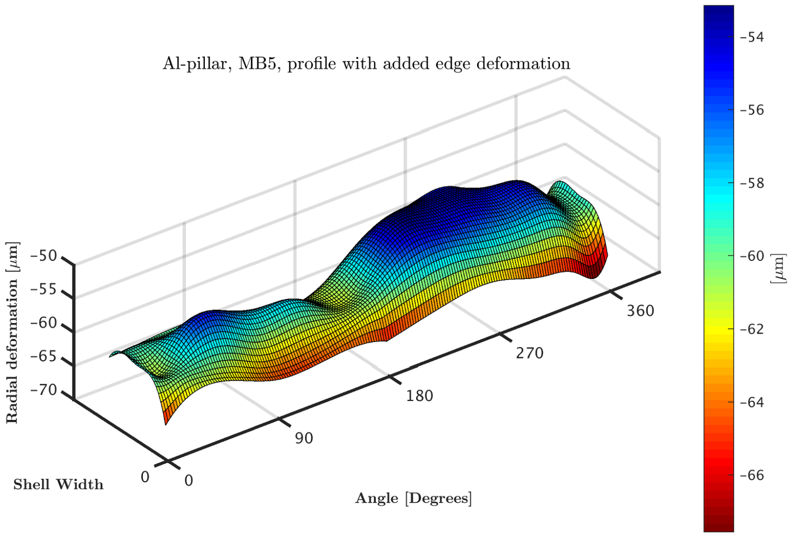

Figure A.5: The radial deformation of the profile of MB5 for *Al-pillar* used in *AVL EXCITE PU*.

A.2 Upper Groove

A.2.1 Main Bearing 1

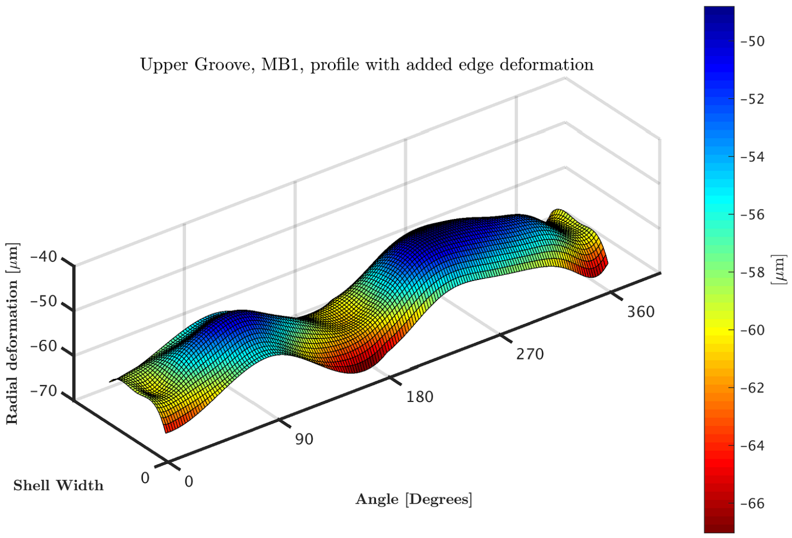

Figure A.6: The radial deformation of the profile of MB1 for *Upper Groove* used in *AVL EXCITE PU*.

A.2.2 Main Bearing 2

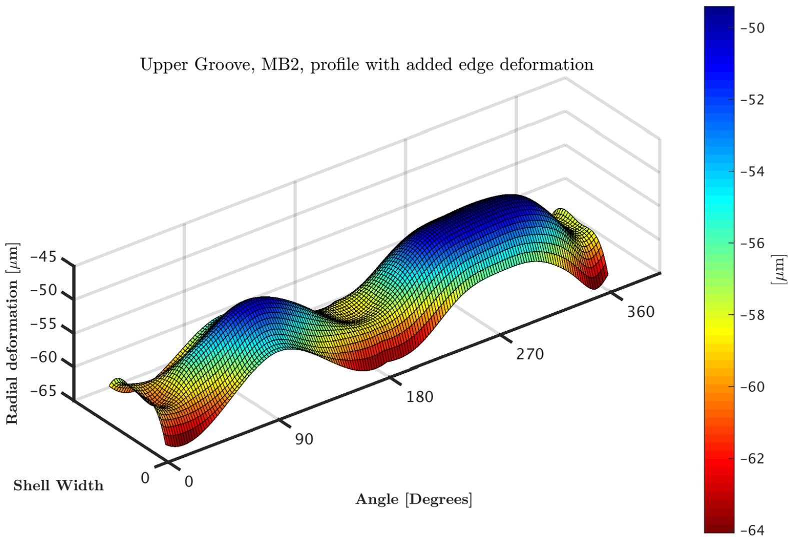

Figure A.7: The radial deformation of the profile of MB2 for *Upper Groove* used in *AVL EXCITE PU*.

A.2.3 Main Bearing 3

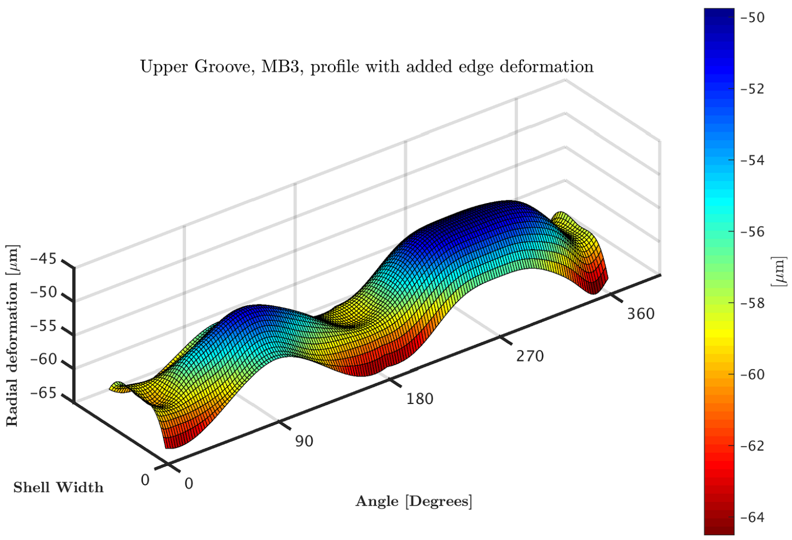

Figure A.8: The radial deformation of the profile of MB3 for *Upper Groove* used in *AVL EXCITE PU*.

A.2.4 Main Bearing 4

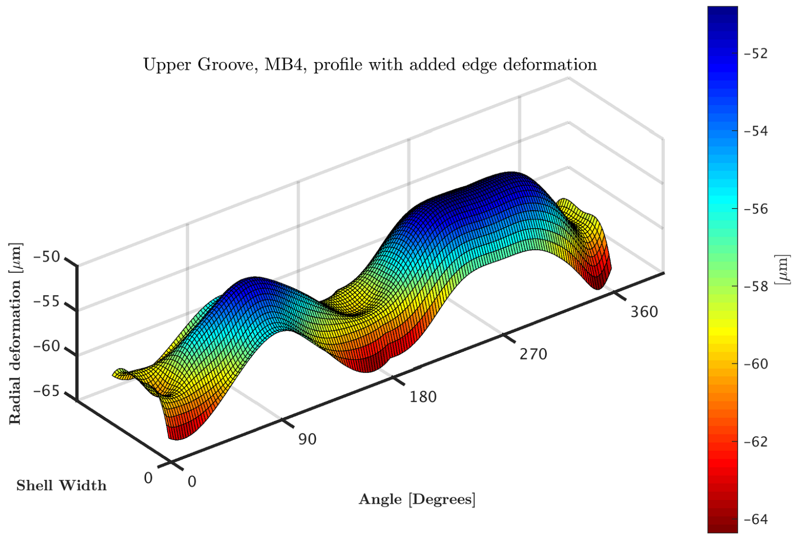

Figure A.9: The radial deformation of the profile of MB4 for *Upper Groove* used in *AVL EXCITE PU*.

A.2.5 Main Bearing 5

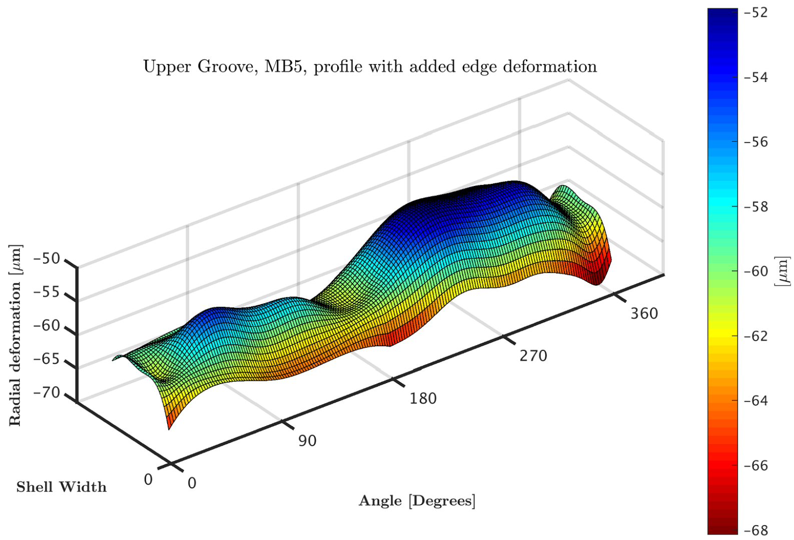

Figure A.10: The radial deformation of the profile of MB5 for *Upper Groove* used in *AVL EXCITE PU*.

A.3 Double Groove

A.3.1 Main Bearing 1

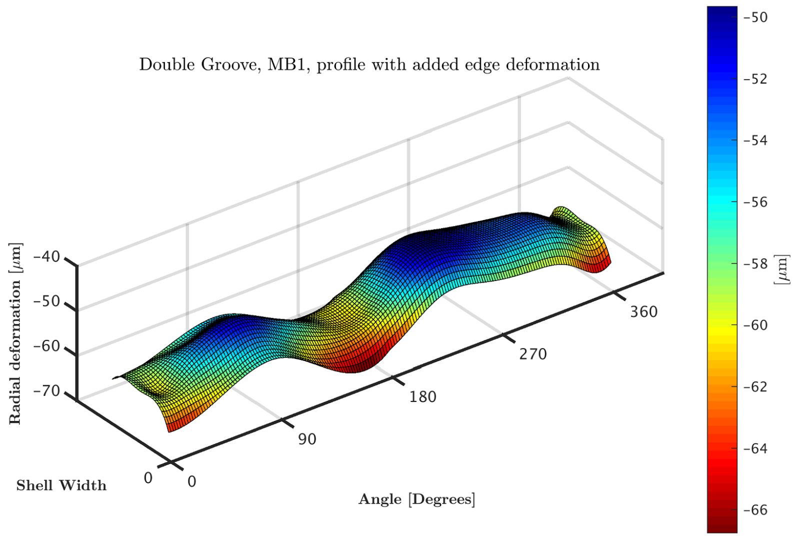

Figure A.11: The radial deformation of the profile of MB1 for *Double Groove* used in *AVL EXCITE PU*.

A.3.2 Main Bearing 2

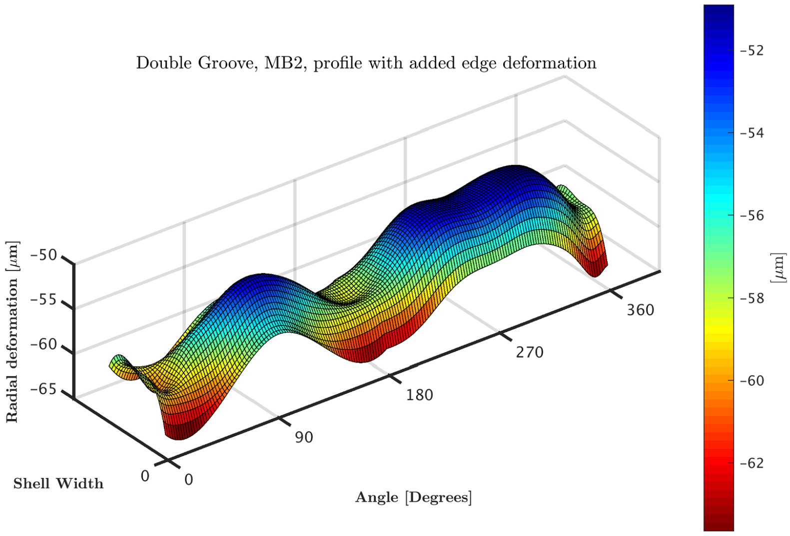

Figure A.12: The radial deformation of the profile of MB2 for *Double Groove* used in *AVL EXCITE PU*.

A.3.3 Main Bearing 3

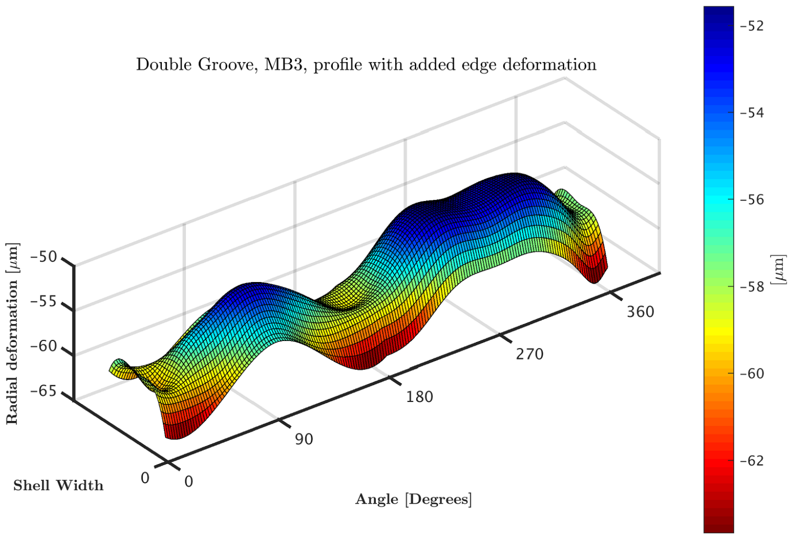

Figure A.13: The radial deformation of the profile of MB3 for *Double Groove* used in *AVL EXCITE PU*.

A.3.4 Main Bearing 4

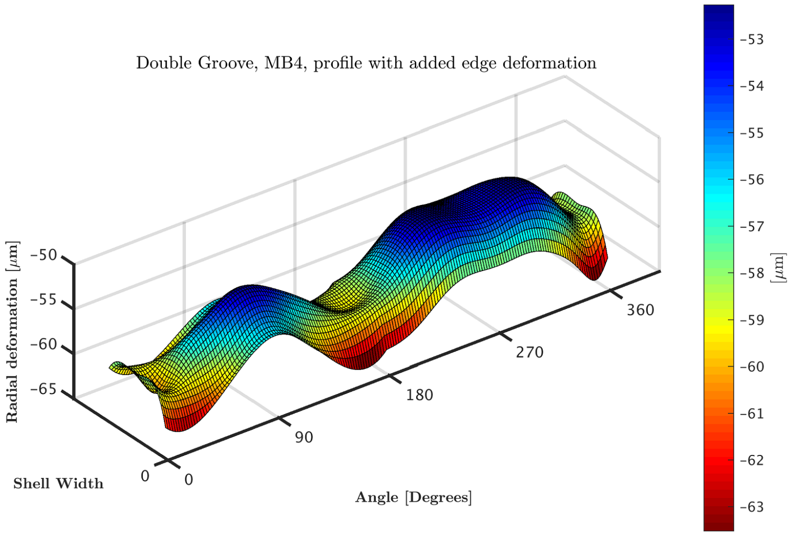

Figure A.14: The radial deformation of the profile of MB4 for *Double Groove* used in *AVL EXCITE PU*.

A.3.5 Main Bearing 5

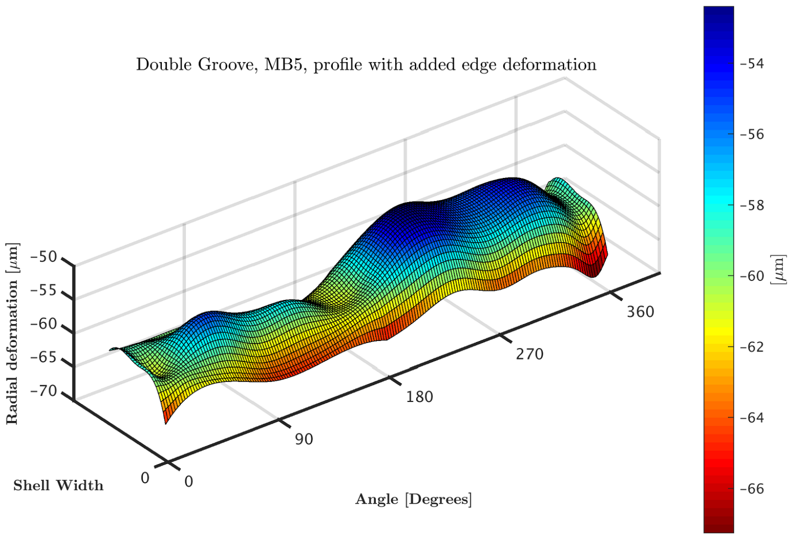

Figure A.15: The radial deformationof the profile of MB5 for *Double Groove* used in *AVL EXCITE PU*.

A.4 Combination of Grooves

A.4.1 Main Bearing 1

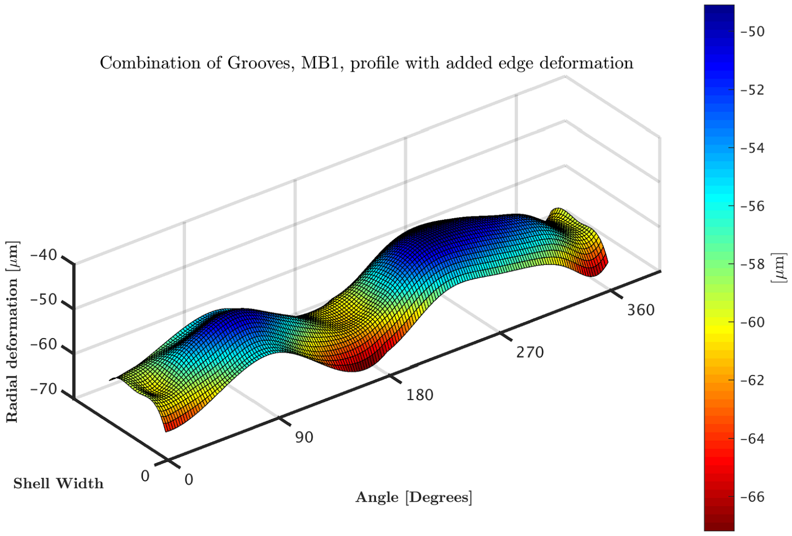

Figure A.16: The radial deformation of the profile of MB1 for *Combination of Grooves* used in *AVL EXCITE PU*.

A.4.2 Main Bearing 2

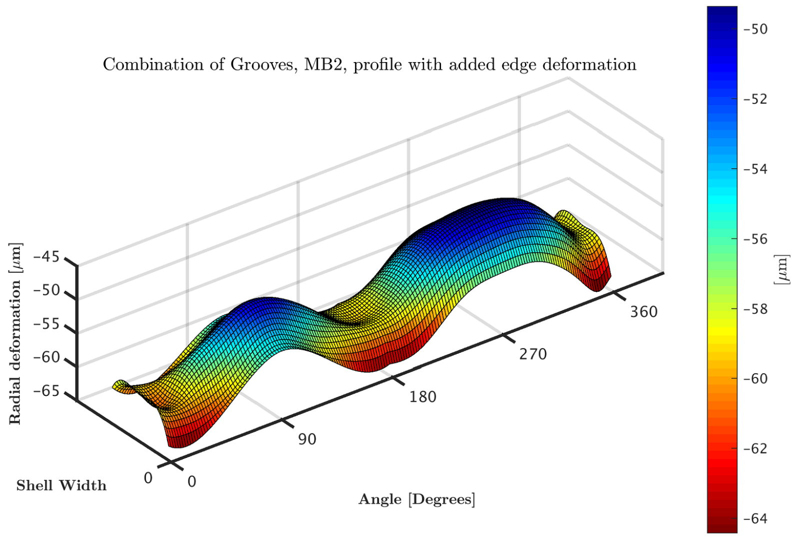

Figure A.17: The radial deformationof the profile of MB2 for *Combination of Grooves* used in *AVL EXCITE PU*.

A.4.3 Main Bearing 3

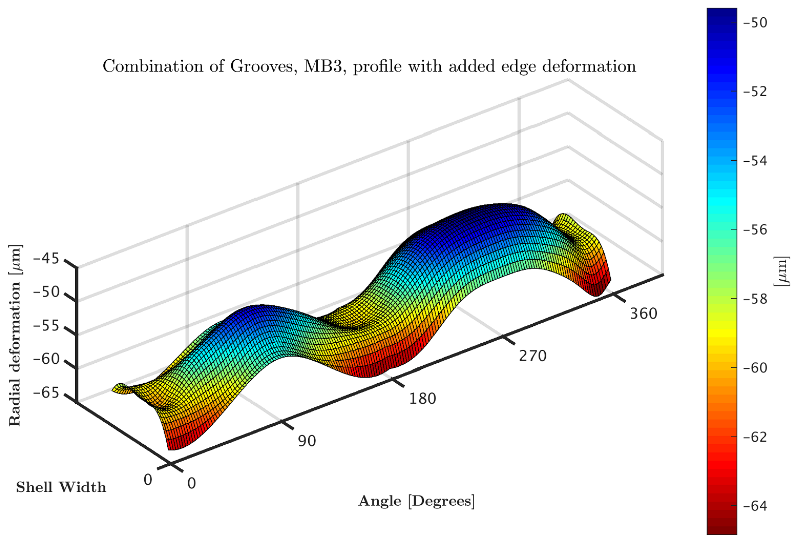

Figure A.18: The radial deformation of the profile of MB3 for *Combination of Grooves* used in *AVL EXCITE PU*.

A.4.4 Main Bearing 4

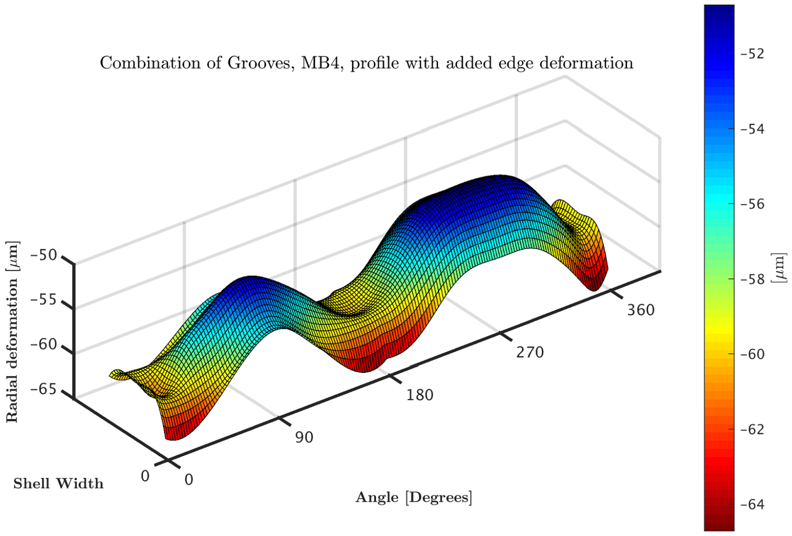

Figure A.19: The radial deformation of the profile of MB4 for *Combination of Grooves* used in *AVL EXCITE PU*.

A.4.5 Main Bearing 5

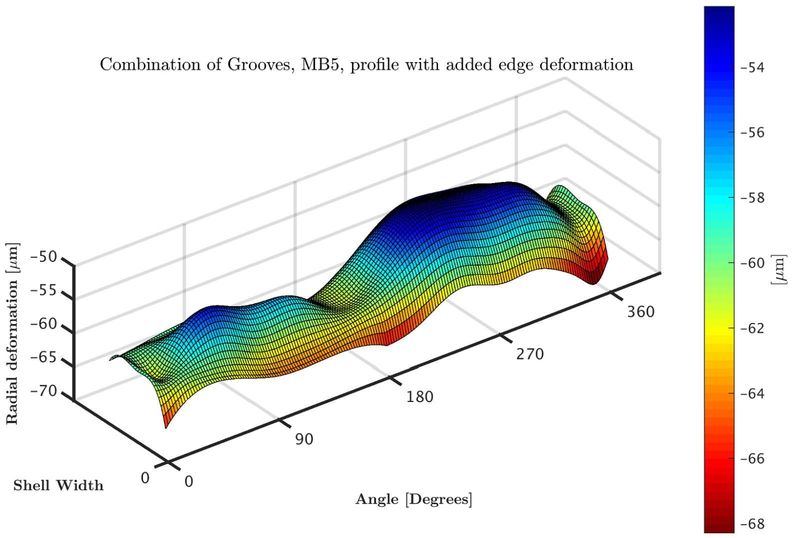

Figure A.20: The radial deformation of the profile of MB5 for *Combination of Grooves* used in *AVL EXCITE PU*.

A.5 Spray

A.5.1 Main Bearing 1

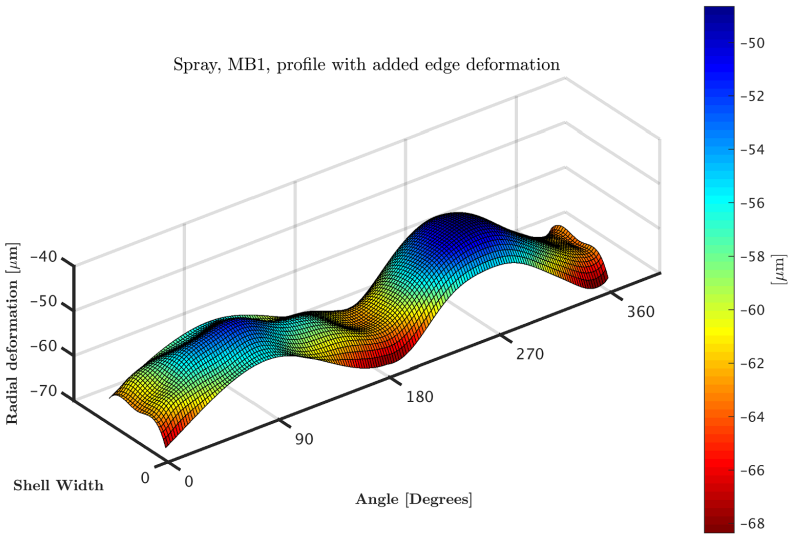

Figure A.21: The radial deformation of the profile of MB1 with a sprayed main bearing support.

A.5.2 Main Bearing 2

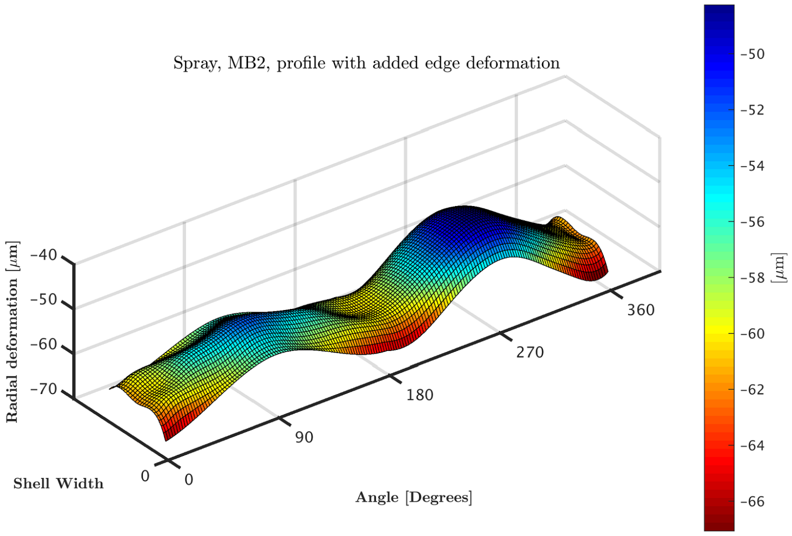

Figure A.22: The radial deformationof the profile of MB2 with a sprayed main bearing support.

A.5.3 Main Bearing 3

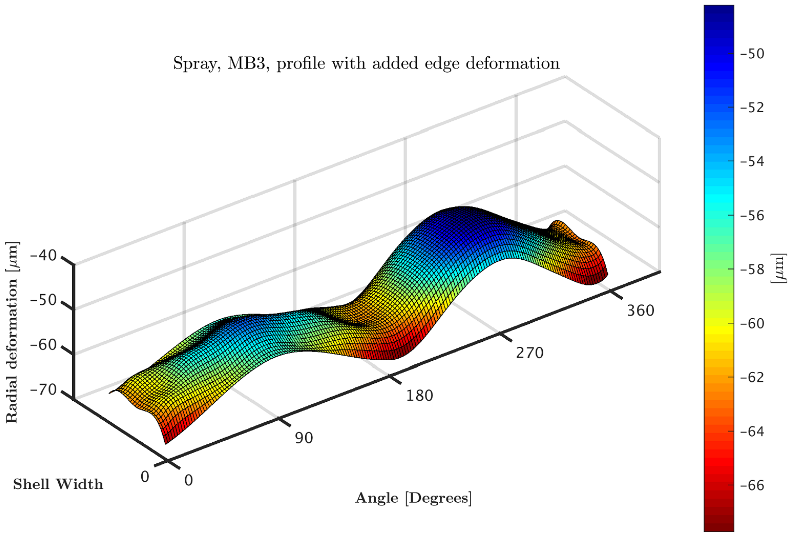

Figure A.23: The radial deformation of the profile of MB3 with a sprayed main bearing support.

A.5.4 Main Bearing 4

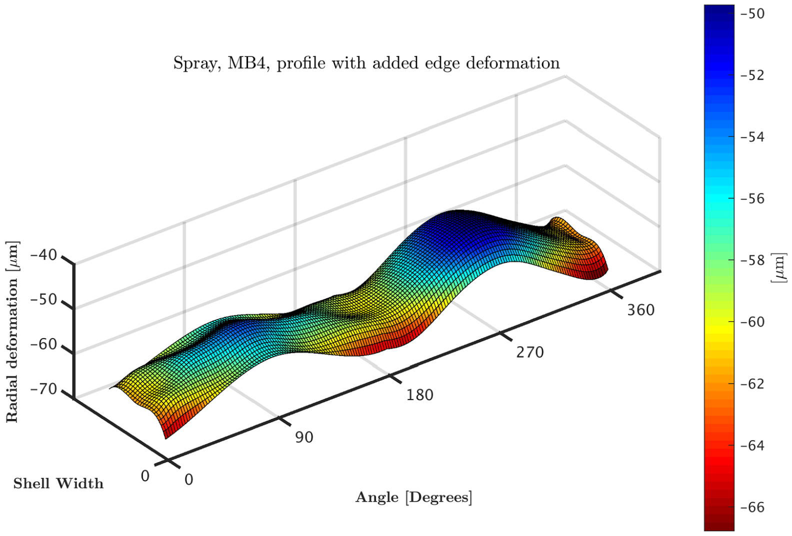

Figure A.24: The radial deformation of the profile of MB4 with a sprayed main bearing support.

A.5.5 Main Bearing 5

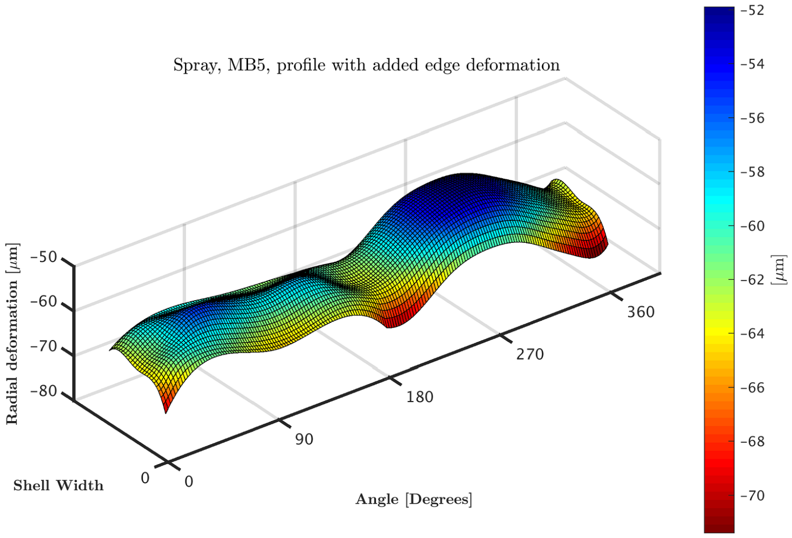

Figure A.25: The radial deformation of the profile of MB5 with a sprayed main bearing support.

B

Maximum total pressure

B.0.1 Maximum total pressure at 1000 rpm

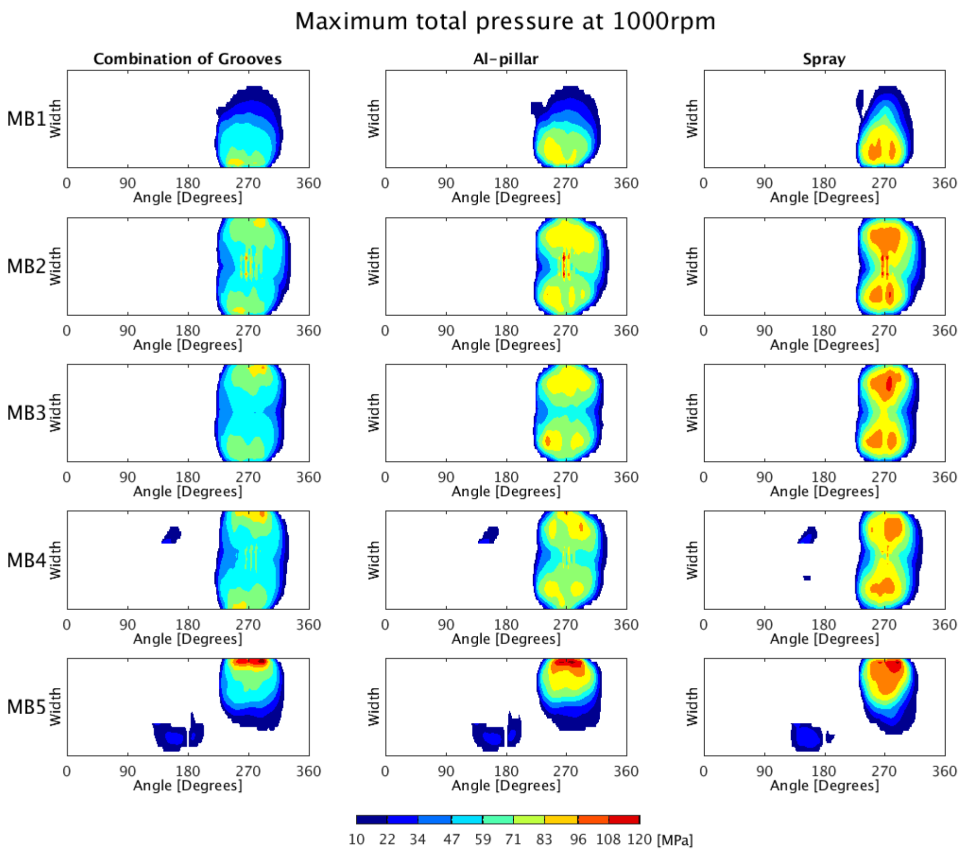

Figure B.1: The maximum total pressure at 1000 rpm shown for all the main bearings unwrapped. Each column represents the designs of the main bearing supports. From left to right is *Combination of Grooves*, *Al-pillar* and *Spray*.

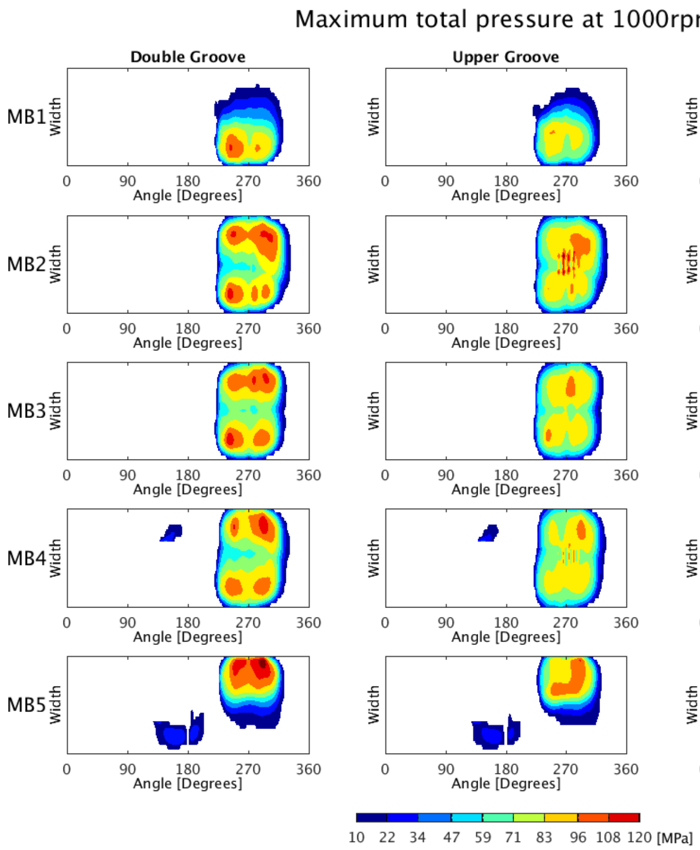

Figure B.2: The maximum total pressure at 1000 rpm shown for all the main bearings unwrapped. Each column represents the designs of the main bearing supports. From left to right is *Upper Groove*, *Double Groove* and *Spray*.

B.0.2 Maximum total pressure at 2000 rpm

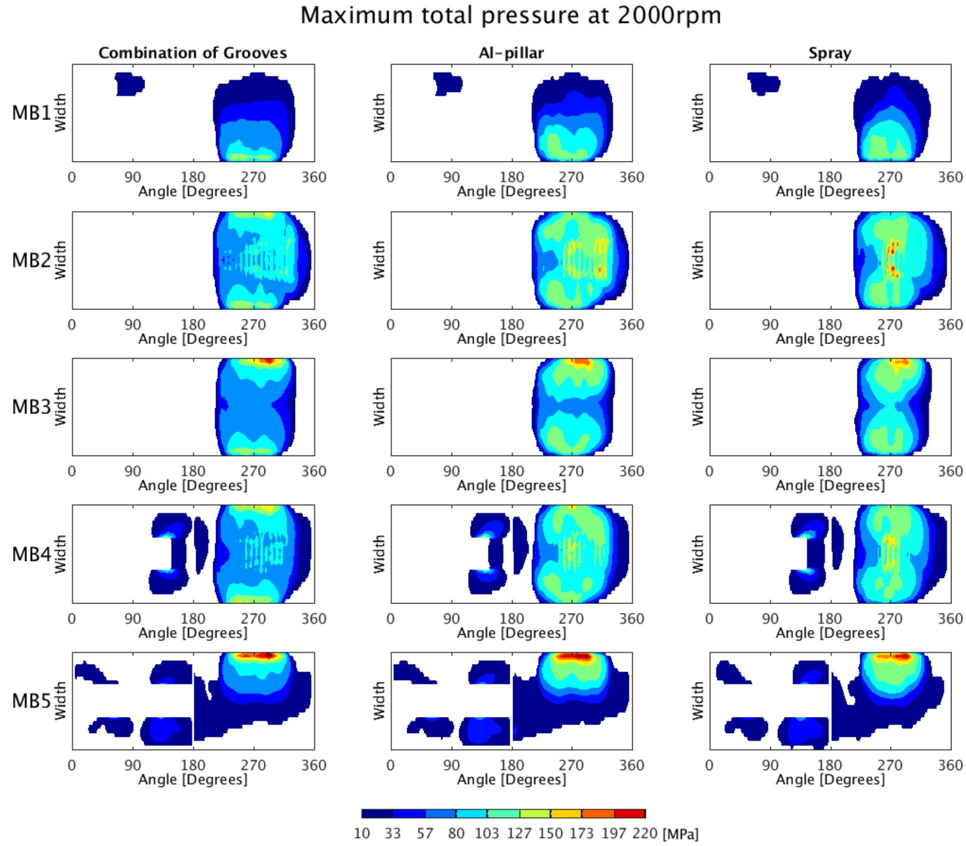

Figure B.3: The maximum total pressure at 2000 rpm shown for all the main bearings unwrapped. Each column represents the designs of the main bearing supports. From left to right is *Combination of Grooves*, *Al-pillar* and *Spray*.

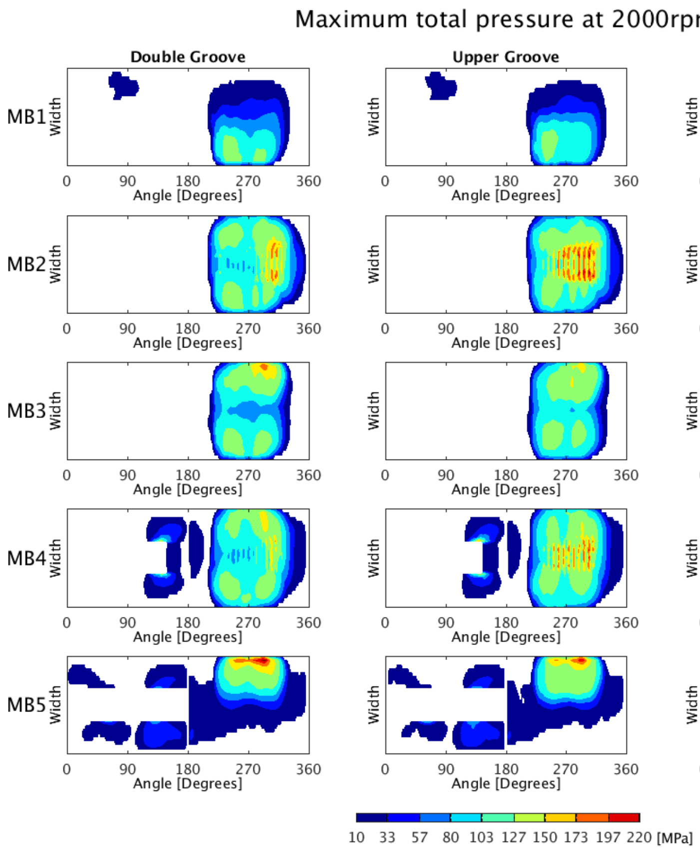

Figure B.4: The maximum total pressure at 2000 rpm shown for all the main bearings unwrapped. Each column represents the designs of the main bearing supports. From left to right is *Upper Groove*, *Double Groove* and *Spray*

B.0.3 Maximum total pressure at 4000 rpm

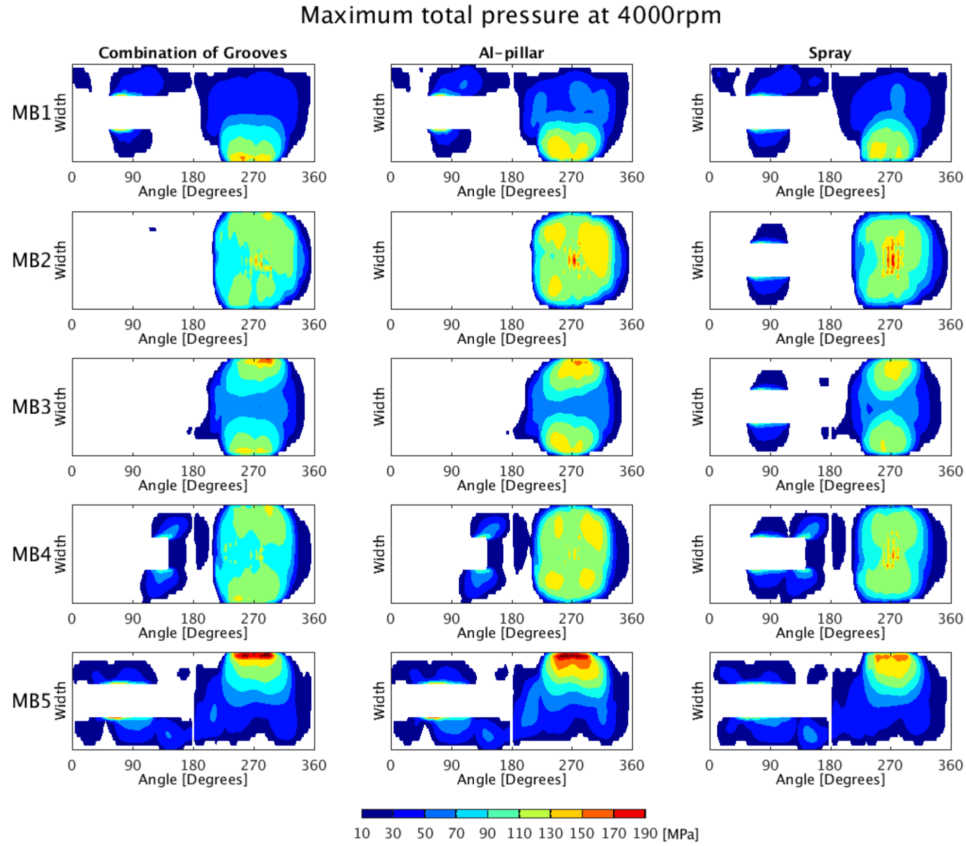

Figure B.5: The maximum total pressure at 4000 rpm shown for all the main bearings unwrapped. Each column represents the designs of the main bearing supports. From left to right is *Combination of Grooves*, *Al-pillar* and *Spray*.

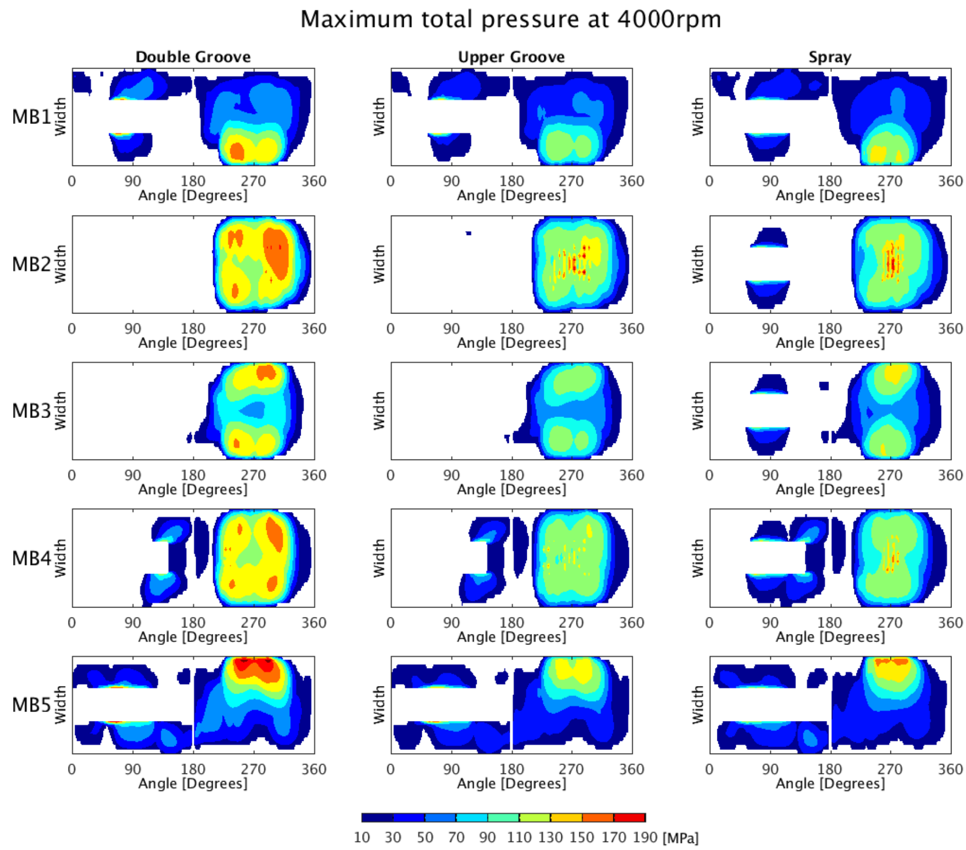

Figure B.6: The maximum total pressure at 4000 rpm shown for all the main bearings unwrapped. Each column represents the designs of the main bearing supports. From left to right is *Upper Groove*, *Double Groove* and *Spray*.